AN OPTIMIZATION-BASED MULTIBODY DYNAMICS MODELING METHOD FOR TEAM LIFTING SIMULATION

By

MD ASIF AREFEEN

Bachelor of Science in Aeronautical Engineering

Bangladesh University of Professionals

Dhaka, Bangladesh

2015

Submitted to the Faculty of the
Graduate College of the
Oklahoma State University
in partial fulfillment of
the requirements for
the Degree of
MASTER OF SCIENCE
December, 2019

AN OPTIMIZATION-BASED MULTIBODY

DYNAMICS MODELING METHOD FOR TEAM

LIFTING SIMULATION

Thesis Approved:

Yujiang Xiang

Thesis Adviser

Jerome G. Hausselle

Shuodao Wang

ACKNOWLEDGEMENTS

Firstly, I would like to extend my deepest gratitude to my advisor Dr. Yujiang Xiang for his continuous support and motivation through each stage of the process.

I would also like to acknowledge Dr. Jerome G. Hausselle and Dr. Shuodao Wang as the committee members of this thesis, and I am thankful to them for their valuable comments on this thesis.

I must thank the National Institute for Occupational Safety and Health (NIOSH) and Southwest Center for Occupational and Environmental Health (SWCOEH) for supporting this research.

Finally, I am extremely grateful to my parents and to my wife, Proapa for providing me with support and continuous encouragement.

Name: MD ASIF AREFEEN

Date of Degree: DECEMBER, 2019

Title of Study: AN OPTIMIZATION-BASED MULTIBODY DYNAMICS MODELING METHOD FOR TEAM LIFTING SIMULATION

Major Field: MECHANICAL ENGINEERING

Abstract: A novel optimization-based multibody dynamics modeling method is proposed for two-dimensional (2D) team lifting prediction. The box itself is modeled as a floating-base rigid body in Denavit-Hartenberg representation. The interactions between humans and box are modeled as a set of grasping forces which are treated as unknowns (design variables) in the optimization formulation. An inverse dynamics optimization is used to simulate the team lifting motion where the dynamic effort of two humans is minimized subjected to physical and task-based constraints. The design variables are control points of cubic B-splines of joint angle profiles of two humans and the box, and the grasping forces between humans and the box. Analytical sensitivities are derived for all constraints and objective functions, including the varying unknown grasping forces. Two numerical examples are successfully simulated: one is to lift a 10 Kg box with the center of mass (COM) in the middle, and the other is the same weight box with the COM off the center. The humans' joint angle, torque, ground reaction force, and grasping force profiles are reported. The optimal solution is obtained in 151.99 seconds. The simulated motions are validated against the experimental joint angle profiles. Reasonable team lifting motion, kinematics, and kinetics are predicted using the proposed novel multibody dynamic modeling approach and optimization formulation.

TABLE OF CONTENTS

Chapter Page

LIST OF TABLES

Table Page

LIST OF FIGURES

Figure Page

Figure Page

CHAPTER I

INTRODUCTION

1.1 Motivation and Objectives

Two-person or team lifting is a popular manual handling strategy that is routinely used when the lifting capacity of the single worker is expected to be exceeded by the lifting tasks and also when mechanical assistance is not available. Due to the variety of lifting situations, it would be difficult to provide a mechanical device, but team lifting can be used in handling heavy and awkward or bulky objects. Team lifting is also often used in the furniture handling industry, manufacturing, and construction sectors (Marras et al., 1999), retails sales, and healthcare industry to transfer patients (Charney et al., 1991, Daynard et al., 2001). In addition, it was reported that 53% of all lifts performed by military personnel were performed by more than one person (Sharp et al., 1997).

The primary objective of this research is to develop a 2D team lifting prediction model to study the cause-and-effect. In addition, the simulation results are validated against the experimental data. The ultimate goal is to develop a subject-specific ergonomic tool to protect workers from injury for team lifting tasks.

1.2 Background

In recent decades, there has been a great amount of work on developing guidelines for manual material handling (MMH) such as NIOSH lifting equations. Many researchers have conducted MMH studies, but these studies were mostly about single person lifting although team lifting tasks are required in many workplaces. The experiment-based physiological, psychophysical, and biomechanical approaches are the three methods for analyzing team lifting in the literature. The only predictive team lifting simulations are in the robotics field to study load sharing problems among robots or between human and robot using optimization (Cheng and Orin, 1991; Lawitzky et al., 2010; DelPreto and Rus, 2019).

The physiological approach is related to the metabolic and circulatory capabilities of the human body. A person's ability to lift during frequent and prolonged tasks may be limited by his/her metabolic and circulatory capabilities. This approach is focused on determining the energy requirements of the task and the effects on the cardiovascular system during MMH tasks (Konz and Johnson, 2004). Metabolic energy expenditure is directly proportional to the workload at steady-state conditions (Aquilano, 1968; Astrand and Rodahl, 1986; Ayoub et al., 1981; Durnin and Passmore, 1967; Hamilton and Chase, 1969; Mital, 1984). The metabolic rate at which body expends energy was considered as the limiting factor when the lifting frequencies were more than eight lifts per minute. This approach was used to determine the expected weight to be lifted (Chaffin et al., 1999). In the case of manual lifting, mathematical models exist to predict motion and maximum lifting weight based on oxygen uptake (Aberg et al., 1967; Frederik, 1959) or energy cost.

The psychophysical approach depends on human feelings, physical strain, discomfort, and fatigue with MMH tasks. In this method, the subjects first estimate the amount of weight that can be lifted comfortably over a specified time period without experiencing any strain or discomfort.

Then lifting experiment is conducted to verify these estimations. For maximum weight lifting, the extreme load is not used in experiments instead the weight is gradually increased until the subjects stop the process to avoid injury. Using the psychophysical method, Karwowski (1988) and Lee and Lee (2001) reported that for infrequent lifting of compact loads by inexperienced and young college students, the best predictor of team lifting capacity was the strength of the strongest team member. On the other hand, some researchers suggested that the best way to predict the team lifting power was the strength of the weakest team member (Rice et al., 1995; Fox, 1982). In the literature, there are some general conclusions for psychophysical method: the maximum lifting capacity for a lifting team is higher than for an individual, males on average have a greater maximum lifting capacity than females, and mixed-gender teams have an intermediate lifting capacity (Karwowski, 1988; Mital and Motorwala, 1995; Sharp et al., 1997). In addition, the maximum lifting capacity for a two-person team was less than the summed lifting capacity of the team members (Karwowski, 1988; Karwowski and Mital, 1986; Karwowski and Pongpatanasuegsa, 1988; Sharp et al., 1997; Lee and Lee, 2001) whereas contradictory findings have been reported by other researchers (Johnson and Lewis, 1989; Mital and Motorwala, 1995). Furthermore, the lifting capacity is decreased when the height of the lifting team members is unmatched (Lee and Lee, 2001). Due to some contradictory findings, the psychophysical studies of team lifting capacity to date are somewhat ambiguous. But, factors like strength, gender, standing height of team members and the nature of the lifting task influence team lifting capacity.

The experiment-based biomechanical approach focuses on determining forces and torques acting on the human body for MMH tasks and their effects on various body parts and joints. Experimental data are first collected including motion capture data, ground reaction forces (GRFs), and electromyography (EMG), then input into the biomechanical model to analyze the lumbar spine compression and shear forces for team lifting motion (Marras et al. 1999). Dennis and Barrett (2003) have examined factors that influence spinal loads in team lifting. For the

matched and unmatched standing height of the team members, taller subjects experienced greater mean spinal loads than the shorter subjects in the unmatched condition compared to the matched condition. In addition, the person at the heavier end of the load experienced higher spinal loads due to the effect of load mass distribution.

Predictive team lifting simulation is a challenging task due to model complexity, unknown grasping forces, and load distribution between subjects. Over the last few decades, researchers developed biomechanical prediction approaches for lifting (Ayoub, 1992; Arisumi et al., 2007; Xiang et al., 2010a, 2010b, 2012; Song et al., 2016), but no work was reported for team lifting predictions. Forward dynamics optimization (Thelen et al., 2006; Shourijeh et al., 2014), inverse dynamics optimization (Fregly et al., 2007; Ren et al., 2007; Xiang et al., 2009a; Farahani et al., 2016), and optimization with direct collocations (Ackermann & Van den Bogert, 2010; Arora & Wang, 2005) are several different optimization formulations for lifting simulations. This research aims to develop a novel optimization-based multibody dynamics modeling method to predict team lifting motion. The simulated results can be used to plan the optimal team lifting motion to protect workers from injury for team lifting tasks.

1.3 Overview of thesis and specific contribution

The thesis contents are organized as follows: the multibody human-box system is first described in Chapter 2, and recursive kinematics and dynamics with sensitivity analysis are developed. Also, new sensitivity equations about varying external force is derived. Chapter 3 covers the details of the optimization formulation including design variables, objective function, and constraints for the team lifting problem. Chapter 4 presents two numerical examples, centric- and eccentric-weight lifting with experimental validations and discussions. Finally, concluding remarks and plan for future research are given in Chapter 5.

The research contributions of this work are summarized as follows:

(1) A novel optimization-based multibody dynamics modeling method was proposed for 2D team lifting prediction and hand grasping forces prediction.

(2) Joint actuating torque was calculated from the inverse recursive Lagrangian dynamics with analytical gradient evaluations in the optimization process so that the formulation was computationally efficient.

(3) The effect of the box center of mass (COM) was investigated. The simulation demonstrated that the box COM location has significant effects on the optimal team lifting strategy, kinematics, and kinetics.

(4) The simulated motion was validated against the experimental joint angle profiles. Reasonable team lifting motion, kinematics, and kinetics were predicted using the proposed novel multibody dynamic modeling approach and optimization formulation. These results can be used to plan the optimal team lifting motion to prevent injury.

CHAPTER II

MULTIBODY HUMAN-BOX SYSTEM

2.1 Human-box Model

Two 2D human skeletal models and a floating-base rigid box are considered in this work as shown in Figure 2.1. The human skeletal model is symmetric along the sagittal plane and has $n = 10$ degrees of freedom (DOFs). The box has three global DOFs including two translations and one rotation. Each human skeletal model consists of two physical branches and one virtual branch including the global DOFs. The two physical branches are the spine-arm branch and leg branch. In the spine-arm branch, two arms are represented by a single branch since only 2D symmetric lifting is studied. The arm branch includes an upper arm and a lower arm. In the leg branch, two legs are combined as a single branch including thigh, tibia, and foot. Both the human skeletal models and the box are constructed by using the well-established robotic formulation of the Denavit-Hartenberg (DH) method (Denavit and Hartenberg, 1955). Each DOF represents relative rotation/translation of two body segments connected by a revolute/prismatic joint. For revolute joints, the direction of rotation is the local z-axis according to the right-hand rule. On the other hand, for prismatic joints, the direction of the movement is the translation along the local z-axis. It is noted that the global rotation joint (z_3), spine joint (z_4), and hip joint (z_7) coincide at the same location for human1, and the global rotation joint (z_{13}), spine joint (z_{14}), and hip joint (z_{17}) coincide at the same location for human2 in Figure 2.1. The positive directions for all the local rotation joints

($z_3 \sim z_{10}$) of human1 and box (z_{23}) are clockwise in the global Y-Z plane, but for the human2 the local rotational joints ($z_{14} \sim z_{20}$) are counter clockwise in the global Y-Z plane. In addition, there are two grasping forces ($\mathbf{f}_1^c$ and $\mathbf{f}_2^c$) acting on the two bottom edges of the box as depicted in Figure 2.1. In this study, human1 and human2's anthropometric data are generated from GEBOD™, a regression-based utility software based on the measured height, weight, and stature (Cheng et al., 1994).

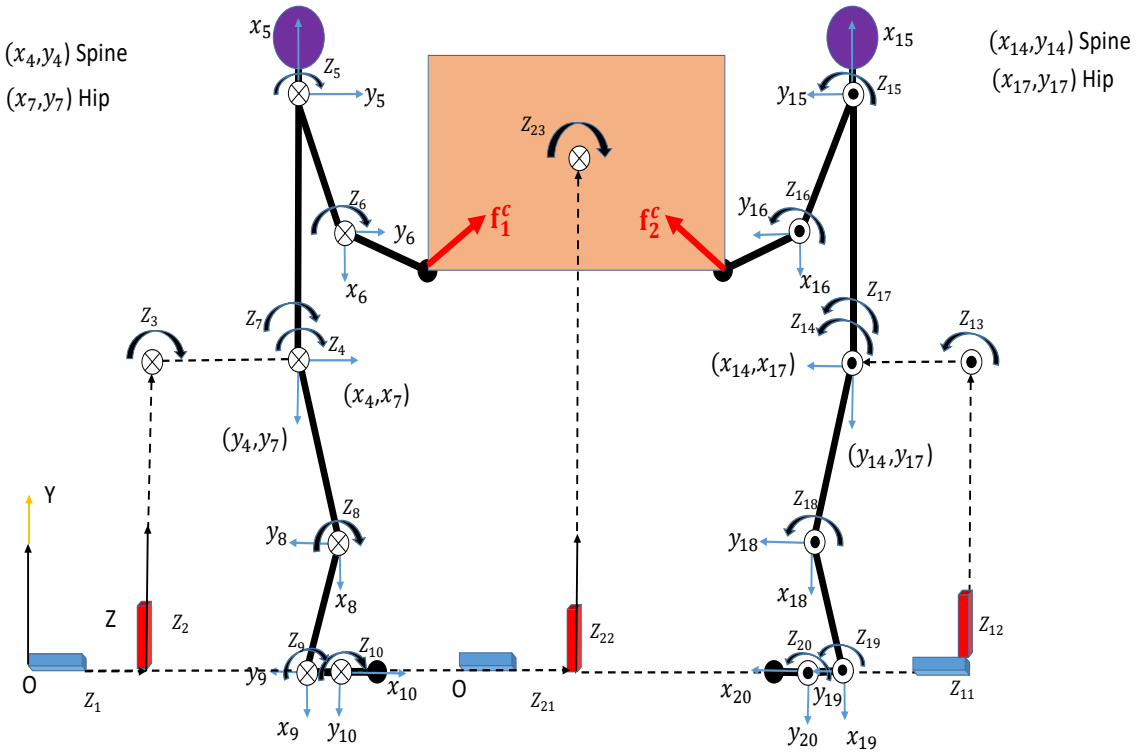

Figure 2.1. The 23-DOF 2D team lifting skeletal-box model (with global DOFs, human1: z_1, z_2, z_3; human2: z_{11}, z_{12}, z_{13}; box: z_{21}, z_{22}, z_{23})

In Figure 2.1 both for human1 and human2, three DOFs are used for global translations and rotation and seven DOFs are for the body joints. Only two global translations and one global rotation are considered for the box, so it is called floating base box.

Table 2.1 Joint angle symbols and names for human1

Symbol	Coordinate name	Symbol	Coordinate name
z_1	Global translation joint coordinate	z_6	Elbow joint coordinate
z_2	Global translation joint coordinate	z_7	Hip joint coordinate
z_3	Global rotation joint coordinate	z_8	Knee joint coordinate
z_4	Spine joint coordinate	z_9	Ankle joint coordinate
z_5	Arm joint coordinate	z_{10}	Subtalar joint coordinate

Table 2.2 Joint angle symbols and names for human2

Symbol	Coordinate name	Symbol	Coordinate name
z_{11}	Global translation joint coordinate	z_{16}	Elbow joint coordinate
z_{12}	Global translation joint coordinate	z_{17}	Hip joint coordinate
z_{13}	Global rotation joint coordinate	z_{18}	Knee joint coordinate
z_{14}	Spine joint coordinate	z_{19}	Ankle joint coordinate
z_{15}	Arm joint coordinate	z_{20}	Subtalar joint coordinate

Table 2.3 Joint angle symbols and names for the Box

Symbol	Coordinate name
z_{21}	Global translation joint coordinate
z_{22}	Global translation joint coordinate
z_{23}	Global rotation joint coordinate

2.1.1 Denavit-Hartenberg (DH) Table

The DH parameters for human1, human2, and the box are described in Table 2.4, 2.5, 2.6 where θ represents a rotation about local z-axis, d represents the translational distance on local z-axis, a represents the translational distance on the local x-axis, and α represents the rotation on the local x-axis. The motion sequence is θ, d, a, and α. As there are two branches in each body frame, each branch has a starting local frame that inherits from its parent branch.

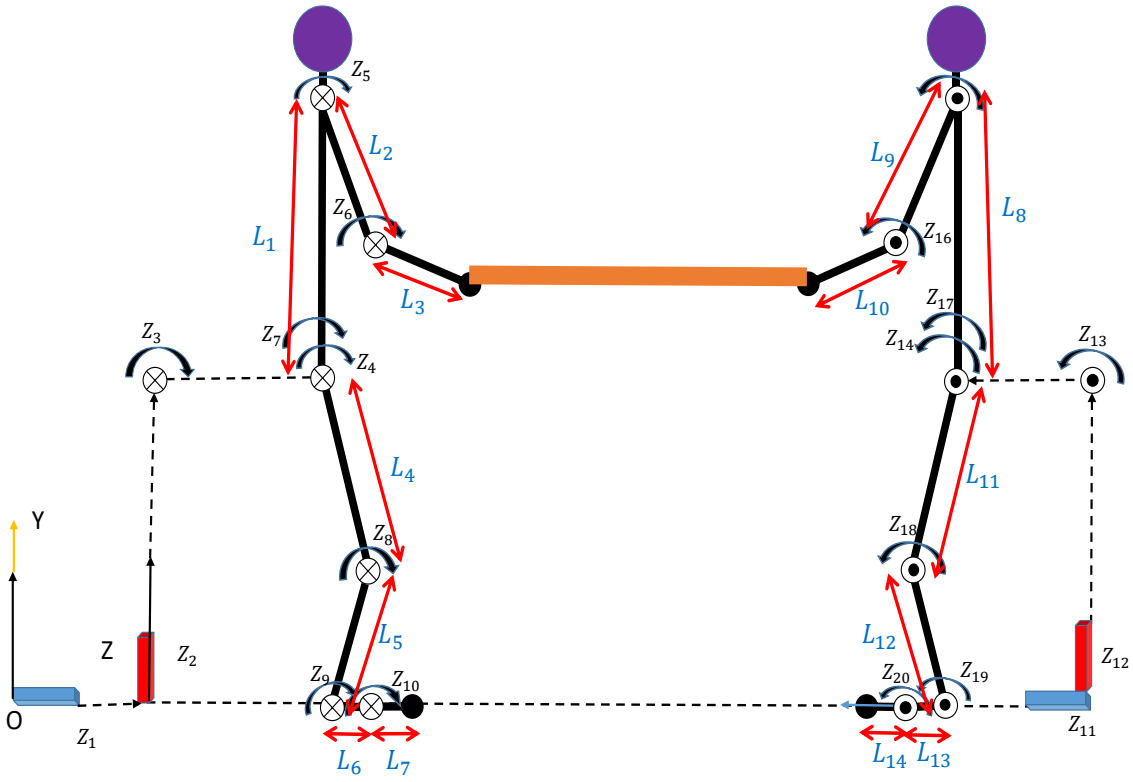

Figure 2.2 Two 2D skeletal models with link lengths

Table 2.4 DH table for 2D human1 model

DOF	Θ	d	a	α
1	π	0	0	$\pi/2$
2	$\pi/2$	L_4+L_5	0	$-\pi/2$
3	0	0	0	0
4	$-\pi/2$	0	L_1	0
5	π	0	L_2	0
6	0	0	L_3	0
7	$\pi/2$	0	L_4	0
8	0	0	L_5	0
9	$-\pi/2$	0	L_6	0
10	0	0	L_7	0

Table 2.5 DH table for 2D human2 model

DOF	Θ	d	a	α
11	π	0	0	$\pi/2$
12	$\pi/2$	L_{11}+L_{12}	0	$\pi/2$
13	0	0	0	0
14	$\pi/2$	0	L_8	0
15	$-\pi$	0	L_9	0
16	0	0	L_{10}	0
17	$-\pi/2$	0	L_{11}	0
18	0	0	L_{12}	0
19	$-\pi/2$	0	L_{13}	0
20	0	0	L_{14}	0

Table 2.6 DH table for Box

DOF	Θ	d	a	α
21	π	0	0	$\pi/2$
22	$\pi/2$	0	0	$-\pi/2$
23	0	0	0	0

The link length, mass, and moment of inertia will be obtained from GEBOD™ software based on the subject's measured body weight and stature.

2.2 Kinematics and dynamics

The Newton-Euler and Lagrangian methods have been studied recently to derive the EOM for multibody human dynamics. Accurate sensitivity of dynamics is needed for the gradient-based optimization algorithm, and it is a key factor to solve the problem efficiently and accurately. But it is generally difficult and tedious to develop the sensitivity equations and their implementation. In this work, recursive kinematics and Lagrangian dynamics are used for kinematics and dynamics analysis of the 2D human model. The process includes two parts: forward kinematics and backward dynamics where forward kinematics disseminates the motion from the root to the end-effectors and backward dynamics transfer the forces from end-effectors to the root.

2.2.1 Forward recursive kinematics

In this forward recursive kinematics process, the global position, velocity and acceleration transformation matrices for the *i*th joint can be defined as $\mathbf{A}_i$, $\mathbf{B}_i$, $\mathbf{C}_i$ respectively where all of them are 4 × 4 matrices. So, the forward joint kinematics are calculated as:

$$\mathbf{A}_i = \mathbf{T}_1\mathbf{T}_2\mathbf{T}_3\cdots\mathbf{T}_i = \mathbf{A}_{i-1}\mathbf{T}_i \tag{2.1}$$

$$\mathbf{B}_i = \dot{\mathbf{A}}_i = \mathbf{B}_{i-1}\mathbf{T}_i + \mathbf{A}_{i-1}\frac{\partial \mathbf{T}_i}{\partial q_i}\dot{q}_i \tag{2.2}$$

$$\mathbf{C}_i = \dot{\mathbf{B}}_i = \ddot{\mathbf{A}}_i = \mathbf{C}_{i-1}\mathbf{T}_i + 2\mathbf{B}_{i-1}\frac{\partial \mathbf{T}_i}{\partial q_i}\dot{q}_i + \mathbf{A}_{i-1}\frac{\partial^2 \mathbf{T}_i}{\partial q_i^2}\dot{q}_i^2 + \mathbf{A}_{i-1}\frac{\partial \mathbf{T}_i}{\partial q_i}\ddot{q}_i \tag{2.3}$$

where q_i, $\dot{q}_i$, $\ddot{q}_i$ are angular displacement, velocity, and acceleration for *i*th joint, $i = 1$ to *n*; $\mathbf{A}_0 = [\mathbf{I}]$ (identity matrix) and $\mathbf{B}_0 = \mathbf{C}_0 = [\mathbf{0}]$; $\mathbf{T}_i$ is the DH transformation matrix from the (*i*-1)th frame to the *i*th frame and it is expressed in Eq. (2.4),

$$ {}^{i-1}\mathbf{T}_i = \begin{bmatrix} \cos\theta_i & -\cos\alpha_i \sin\theta_i & \sin\alpha_i \sin\theta_i & a_i \cos\theta_i \\ \sin\theta_i & \cos\alpha_i \cos\theta_i & -\sin\alpha_i \cos\theta_i & a_i \sin\theta_i \\ 0 & \sin\alpha_i & \cos\alpha_i & d_i \\ 0 & 0 & 0 & 1 \end{bmatrix} \tag{2.4} $$

Then the following formulas are used to calculate the global position, velocity, and acceleration of a point in the Cartesian coordinate system.

$$ {}^0\mathbf{r}_i = \mathbf{A}_i \mathbf{r}_i, \qquad {}^0\dot{\mathbf{r}}_i = \mathbf{B}_i \mathbf{r}_i, \qquad {}^0\ddot{\mathbf{r}}_i = \mathbf{C}_i \mathbf{r}_i, \tag{2.1} $$

where ${}^0\mathbf{r}_i$ and $\mathbf{r}_i$ are global and local augmented coordinates, respectively.

2.2.1.1 Kinematics sensitivity analysis

The sensitivity of position, velocity, and acceleration with respect to state variables are given as:

$$ \frac{\partial \mathbf{A}_i}{\partial q_k} = \begin{cases} \dfrac{\partial \mathbf{A}_{i-1}}{\partial q_k}\mathbf{T}_i & (k < i) \\ \mathbf{A}_{i-1}\dfrac{\partial \mathbf{T}_i}{\partial q_k} & (k = i) \\ 0 & (k > i) \end{cases} \tag{2.2} $$

$$ \frac{\partial \mathbf{B}_i}{\partial q_k} = \begin{cases} \dfrac{\partial \mathbf{B}_{i-1}}{\partial q_k}\mathbf{T}_i + \dfrac{\partial \mathbf{A}_{i-1}}{\partial q_k}\dfrac{\partial \mathbf{T}_i}{\partial q_i}\dot{q}_i & (k < i) \\ \mathbf{B}_{i-1}\dfrac{\partial \mathbf{T}_i}{\partial q_k} + \mathbf{A}_{i-1}\dfrac{\partial^2 \mathbf{T}_i}{\partial q_k^2}\dot{q}_i & (k = i) \\ 0 & (k > i) \end{cases} \tag{2.3} $$

$$ \frac{\partial \mathbf{B}_i}{\partial \dot{q}_k} = \begin{cases} \dfrac{\partial \mathbf{B}_{i-1}}{\partial \dot{q}_k}\mathbf{T}_i & (k < i) \\ \mathbf{A}_{i-1}\dfrac{\partial \mathbf{T}_i}{\partial q_k} & (k = i) \\ 0 & (k > i) \end{cases} \tag{2.4} $$

$$ \frac{\partial \mathbf{C}_i}{\partial q_k} = \begin{cases} \dfrac{\partial \mathbf{C}_{i-1}}{\partial q_k}\mathbf{T}_i + 2\dfrac{\partial \mathbf{B}_{i-1}}{\partial q_k}\dfrac{\partial \mathbf{T}_i}{\partial q_i}\dot{q}_i + \dfrac{\partial \mathbf{A}_{i-1}}{\partial q_k}\dfrac{\partial^2 \mathbf{T}_i}{\partial q_i^2}\dot{q}_i^2 + \dfrac{\partial \mathbf{A}_{i-1}}{\partial q_k}\dfrac{\partial \mathbf{T}_i}{\partial q_i}\ddot{q}_i & (k < i) \\ \mathbf{C}_{i-1}\dfrac{\partial \mathbf{T}_i}{\partial q_k} + 2\mathbf{B}_{i-1}\dfrac{\partial^2 \mathbf{T}_i}{\partial q_k^2}\dot{q}_i + \mathbf{A}_{i-1}\dfrac{\partial^3 \mathbf{T}_i}{\partial q_k^3}\dot{q}_i^2 + \mathbf{A}_{i-1}\dfrac{\partial^2 \mathbf{T}_i}{\partial q_k^2}\ddot{q}_i & (k = i) \\ 0 & (k > i) \end{cases} \tag{2.5} $$

$$\frac{\partial \mathbf{C}_i}{\partial \dot{q}_k} = \begin{cases} \dfrac{\partial \mathbf{C}_{i-1}}{\partial \dot{q}_k}\mathbf{T}_i + 2\dfrac{\partial \mathbf{B}_{i-1}}{\partial \dot{q}_k}\dfrac{\partial \mathbf{T}_i}{\partial q_i}\dot{q}_i & (k < i) \\ 2\mathbf{B}_{i-1}\dfrac{\partial \mathbf{T}_i}{\partial q_k} + 2\mathbf{A}_{i-1}\dfrac{\partial^2 \mathbf{T}_i}{\partial q_k^2}\dot{q}_i & (k = i) \\ 0 & (k > i) \end{cases} \tag{2.6}$$

$$\frac{\partial \mathbf{C}_i}{\partial \ddot{q}_k} = \begin{cases} \dfrac{\partial \mathbf{C}_{i-1}}{\partial \ddot{q}_k}\mathbf{T}_i & (k < i) \\ \mathbf{A}_{i-1}\dfrac{\partial \mathbf{T}_i}{\partial q_k} & (k = i) \\ 0 & (k > i) \end{cases} \tag{2.7}$$

2.2.2 Backward recursive dynamics

Based on the forward recursive kinematics, the backward recursive dynamics are expressed in Eqs. (2.12-2.16)

$$\tau_i = \mathrm{tr}\left(\frac{\partial \mathbf{A}_i}{\partial q_i}\mathbf{D}_i\right) - \mathbf{g}^{\mathrm{T}}\frac{\partial \mathbf{A}_i}{\partial q_i}\mathbf{E}_i - \mathbf{f}_k^{\mathrm{T}}\frac{\partial \mathbf{A}_i}{\partial q_i}\mathbf{F}_i - \mathbf{G}_i^{\mathrm{T}}\mathbf{A}_{i-1}\mathbf{z}_0 \tag{2.12}$$

$$\mathbf{D}_i = \mathbf{I}_i\mathbf{C}_i^{\mathrm{T}} + \mathbf{T}_{i+1}\mathbf{D}_{i+1} \tag{2.13}$$

$$\mathbf{E}_i = m_i\mathbf{r}_i + \mathbf{T}_{i+1}\mathbf{E}_{i+1} \tag{2.14}$$

$$\mathbf{F}_i = \mathbf{r}_k\delta_{ik} + \mathbf{T}_{i+1}\mathbf{F}_{i+1} \tag{2.15}$$

$$\mathbf{G}_i = \mathbf{h}_k\delta_{ik} + \mathbf{G}_{i+1} \tag{2.16}$$

where in the Eq. (2.12) the first term is the inertia and Coriolis torque, the second term is the torque due to gravity load, the third term is the torque due to external force, and the fourth term represents the torque due to external moment.

Also, $tr(\cdot)$ is the trace of a matrix, $\mathbf{A}_i$ and $\mathbf{C}_i$ are global position and acceleration transformation matrices, $\mathbf{I}_i$ is the inertia matrix for link *i*, $\mathbf{D}_i$ is the recursive inertia and Coriolis matrix, $\mathbf{E}_i$ is the recursive vector for gravity torque calculation, $\mathbf{F}_i$ is the recursive vector for external force-torque calculation, $\mathbf{G}_i$ is the recursive vector for external moment torque calculation, $\mathbf{g}$ is the gravity vector, m_i is the mass of link *i*, $\mathbf{r}_i$ is the COM of link *i* in the *i*th local frame,

$\mathbf{f}_k = [0 \quad f_{ky} \quad f_{kz} \quad 0]^{\mathrm{T}}$ is the external force applied on link *k*, $\mathbf{r}_k$ is the position of the external force in the *k*th local frame, $\mathbf{h}_k = [h_x \quad 0 \quad 0 \quad 0]^{\mathrm{T}}$ is the external moment applied on link *k*, $\mathbf{z}_0 = [0 \quad 0 \quad 1 \quad 0]^{\mathrm{T}}$ is for a revolute joint, $\mathbf{z}_0 = [0 \quad 0 \quad 0 \quad 0]^{\mathrm{T}}$ is for a prismatic joint, finally, δ_{ik} is Kronecker delta, and the starting conditions are $\mathbf{D}_{n+1} = [\mathbf{0}]$ and $\mathbf{E}_{n+1} = \mathbf{F}_{n+1} = \mathbf{G}_{n+1} = [\mathbf{0}]$.

2.2.3 EOM of floating-base box

The box only has three global DOFs (z_{21}, z_{22}, z_{23}) as shown in Figure 2.1, so it is called a floating-base box. During the lifting process, the grasping forces from human1 and human2 keep the box in balance with the inertia and gravity forces as below,

$$\tau_i = \mathrm{tr}\left(\frac{\partial \mathbf{A}_i}{\partial q_i}\mathbf{D}_i\right) - \mathbf{g}^{\mathrm{T}}\frac{\partial \mathbf{A}_i}{\partial q_i}\mathbf{E}_i - \mathbf{f}_k^{\mathrm{T}}\frac{\partial \mathbf{A}_i}{\partial q_i}\mathbf{F}_i = 0, \qquad i = 1, 2, 3 \tag{2.17}$$

2.2.4 Sensitivity with respect to state variables

The derivatives $\frac{\partial \tau_i}{\partial q_k}$,$\frac{\partial \tau_i}{\partial \dot{q}_k}$, $\frac{\partial \tau_i}{\partial \ddot{q}_k}$ (i = 1 to n; k = 1 to n), can be evaluated in a recursive way using the foregoing recursive Lagrangian dynamics formulation for the human mechanical system as follows (Xiang et al., 2009b):

$$\frac{\partial \tau_i}{\partial q_k} = \begin{cases} tr\left(\frac{\partial^2 \mathbf{A}_i}{\partial q_i \partial q_k}\mathbf{D}_i + \frac{\partial \mathbf{A}_i}{\partial q_i}\frac{\partial \mathbf{D}_i}{\partial q_k}\right) - \mathbf{g}^{\mathrm{T}}\frac{\partial^2 \mathbf{A}_i}{\partial q_i \partial q_k}\mathbf{E}_i - \mathbf{f}^{\mathrm{T}}\frac{\partial^2 \mathbf{A}_i}{\partial q_i \partial q_k}\mathbf{F}_i - \mathbf{G}_i^{\mathrm{T}}\frac{\partial \mathbf{A}_{i-1}}{\partial q_k}\mathbf{z}_0 & (k \le i) \\ tr\left(\frac{\partial \mathbf{A}_i}{\partial q_i}\frac{\partial \mathbf{D}_i}{\partial q_k}\right) - \mathbf{g}^{\mathrm{T}}\frac{\partial \mathbf{A}_i}{\partial q_i}\frac{\partial \mathbf{E}_i}{\partial q_k} - \mathbf{f}^{\mathrm{T}}\frac{\partial \mathbf{A}_i}{\partial q_i}\frac{\partial \mathbf{F}_i}{\partial q_k} & (k > i) \end{cases} \tag{2.18}$$

$$\frac{\partial \tau_i}{\partial \dot{q}_k} = tr\left(\frac{\partial \mathbf{A}_i}{\partial q_i}\frac{\partial \mathbf{D}_i}{\partial \dot{q}_k}\right) \tag{2.19}$$

$$\frac{\partial \tau_i}{\partial \ddot{q}_k} = tr\left(\frac{\partial \mathbf{A}_i}{\partial q_i}\frac{\partial \mathbf{D}_i}{\partial \ddot{q}_k}\right) \tag{2.20}$$

2.2.5 Zero moment point (ZMP) and ground reaction force (GRF)

Zero moment point (ZMP) is a well-known bipedal dynamic stability criterion that has been used widely in the literature. It is defined as the point on the ground at which the resultant tangential moments are zero (Vukobratovic and Borovac, 2004 "zero-moment point, 35 years of its life"). An active-passive algorithm is used to calculate ZMP and GRF to obtain the real joint torque for the multibody human system (Xiang et al., 2009 "one step walking paper"). The algorithm is outlined here as follows:

(1) Given the state variables q_i, $\dot{q}_i$, $\ddot{q}_i$ (design variables) for each DOF, the global resultant active forces ($\mathbf{M}^o, \mathbf{F}^o$) at the origin in the inertial reference frame (Figure 2.1) are obtained from equations of motion without GRF using inverse dynamics.

(2) After that, the ZMP position is calculated from its definition using the global resultant active force as follows:

$$y_{zmp} = 0; \qquad x_{zmp} = 0\,; \qquad z_{zmp} = \frac{-M_x^o}{F_y^o} \tag{2.21}$$

where $\mathbf{M}^o = [M_x^o \;\; 0 \;\; 0]^{\mathrm{T}}$ and $\mathbf{F}^o = [0 \;\; F_y^o \;\; F_z^o]^{\mathrm{T}}$. In addition, the two feet are assumed on the level ground.

(3) After obtaining the ZMP position, the resultant active forces at ZMP ($\mathbf{M}^{zmp}, \mathbf{F}^{zmp}$) are computed using the equilibrium condition as follows:

$$\mathbf{M}^{zmp} = \mathbf{M}^o + \mathbf{F}^o \times {}^o\mathbf{r}_{zmp} \tag{2.22}$$

$$\mathbf{F}^{zmp} = \mathbf{F}^o$$

where ${}^o\mathbf{r}_{zmp}$ is the ZMP position in the global coordinate system obtained from Eq. (2.21).

(4) Then the value and location of GRF are calculated from the equilibrium between the resultant active forces and passive forces at the ZMP:

$$\mathbf{M}^{GRF} + \mathbf{M}^{zmp} = \mathbf{0} \tag{2.23}$$

$$\mathbf{F}^{GRF} + \mathbf{F}^{zmp} = \mathbf{0}$$

$$^{o}\mathbf{r}_{GRF} - {}^{o}\mathbf{r}_{zmp} = \mathbf{0}$$

where $\mathbf{M}^{GRF} = [M_x^{GRF} \quad 0 \quad 0\,]^{\mathrm{T}}$ and $\mathbf{F}^{GRF} = [0 \;\; F_y^{GRF} F_z^{GRF}]^{\mathrm{T}}$.

2.2.6 Sensitivity with respect to varying external force

External forces can be given as constant or varying values in Eqs. (2.12-2.16). In this study, the grasping external forces between human and box are treated as unknowns (design variables) in the optimization formulation. Therefore, the joint torques from the EOM are not only the function of state variables q, but also the varying external forces. The sensitivity of joint torque with respect to external force should be derived for gradient-based optimization. Without loss of generality, an active external load along the vertical direction f_{ky} is treated as a design variable. f_{ky} affects the joint torques in two ways: explicit effect (τ_i^o) from the EOM, and implicit effect ($\tau_i^{\sim}$) from passive GRF. The direct differentiation of τ_i^o with respect to f_{ky} can be obtained from Eq. (2.12) directly as:

$$\frac{\partial \tau_i^o}{\partial f_{ky}} = [0 \quad 1 \quad 0 \quad 0] \frac{\partial \mathbf{A}_i}{\partial q_i} \mathbf{F}_i \tag{2.24}$$

However, the external force, GRF, also depends on f_{ky} passively due to balance condition. In this study, the GRF is calculated from human global joint torques using an active-passive algorithm (Xiang et al., 2009a), as shown in Figure 2.3.

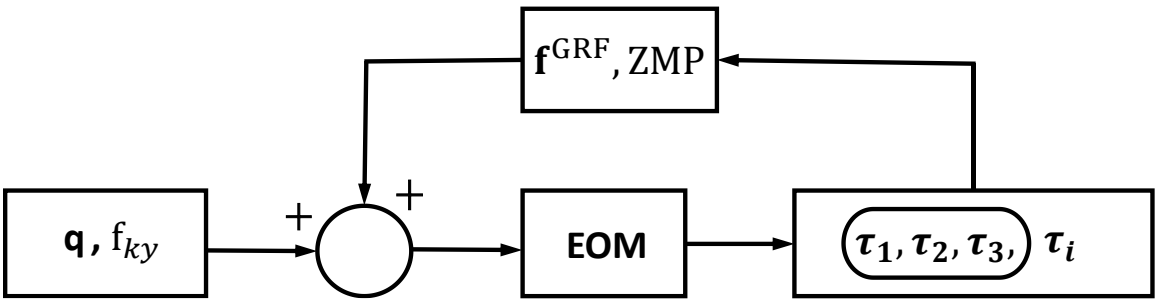

Figure 2.3 GRF active-passive feedback flowchart

Therefore, $\mathbf{f}^{GRF} = [0, \quad f_y^{GRF}(\tau_{1\sim3}^o), \quad f_z^{GRF}(\tau_{1\sim3}^o), \quad 0]^{\mathrm{T}}$ is a function of $\tau_{1\sim3}^o$ (active global joint torques).Then the sensitivity of joint torque $\tau_i^{\sim}$ with respect to f_{ky} due to GRF is calculated using the chain rule as:

$$\frac{\partial \tau_i^{\sim}}{\partial f_{ky}} = \frac{\partial \tau_i^{\sim}}{\partial f_y^{GRF}} \frac{\partial f_y^{GRF}}{\partial \tau_{1\sim3}^o} \frac{\partial \tau_{1\sim3}^o}{\partial f_{ky}} + \frac{\partial \tau_i^{\sim}}{\partial f_z^{GRF}} \frac{\partial f_z^{GRF}}{\partial \tau_{1\sim3}^o} \frac{\partial \tau_{1\sim3}^o}{\partial f_{ky}} \tag{2.25}$$

$$\frac{\partial \tau_i^{\sim}}{\partial f_y^{GRF}} = [0 \quad 1 \quad 0 \quad 0] \frac{\partial \mathbf{A}_i}{\partial q_i} \mathbf{F}_i \tag{2.26}$$

$$\frac{\partial \tau_i^{\sim}}{\partial f_z^{GRF}} = [0 \quad 0 \quad 1 \quad 0] \frac{\partial \mathbf{A}_i}{\partial q_i} \mathbf{F}_i \tag{2.27}$$

where the term $\frac{\partial f_y^{GRF}}{\partial \tau_{1\sim3}^o}$ involves the zero-moment-point (ZMP) location calculation, refer to Section 2.2.5 for detailed calculations. The term $\frac{\partial \tau_{1\sim3}^o}{\partial f_{ky}}$ is obtained from Eq. (2.24). Finally, the sensitivity of the joint torque with respect to the active external load f_{ky} is the summation of Eqs. (2.24) and (2.25):

$$\frac{\partial \tau_i}{\partial f_{ky}} = \frac{\partial \tau_i^o}{\partial f_{ky}} + \frac{\partial \tau_i^{\sim}}{\partial f_{ky}} \tag{2.28}$$

CHAPTER III

FORMULATION

3.1 Team lifting task

In this thesis, the team lifting task is illustrated as moving a box from an initial location to a final location. Figure 3.1 depicts the input parameters for the proposed formulation.

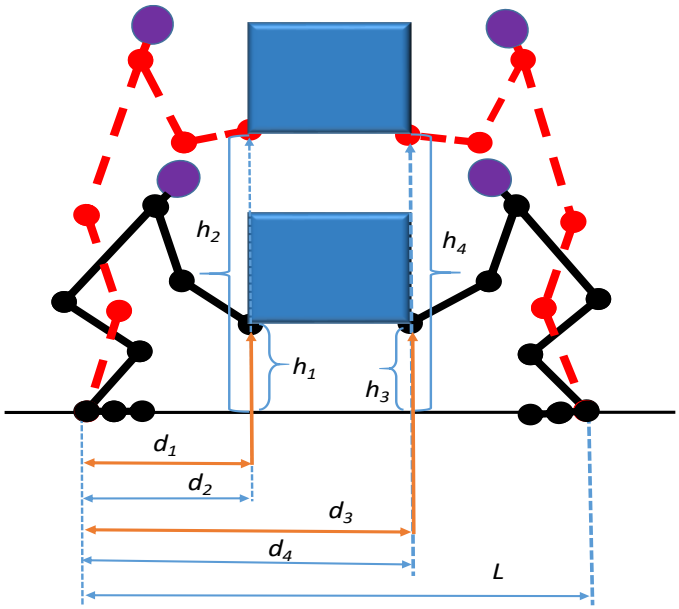

Figure 3.1 Input parameters for the team lifting task

In this regard, h_1 and h_2 are the initial and final heights of the box measured from the ground to the left edge of the box for human1; d_1 and d_2 are the initial and the final hand distance measured from the human1 ankle location to the left edge of the box (side close to human1); h_3 and h_4 are

the initial and final heights for human2 measured from the ground, d_3 and d_4 are the initial and the final hand distance for human2 measured from the human1 ankle location to the right edge (side close to human2) of the box and L is the standing distance (ankle to ankle) between two humans. The dynamic lifting trajectory and grasping forces are solved from a nonlinear optimization problem. In addition, the mechanical system is at rest at the initial and final time points.

3.2 Optimization formulation

The lifting motion is predicted by solving a nonlinear optimization problem. Here the box initial and final positions, the feet positions, and the box dimension and weight are given. The total time T for lifting motion is specified. The joint angles of knee, spine, and elbow at initial, mid-time, final time points are specified from experiments to predict subject-specific lifting strategies.

3.2.1 Design variables

As the lifting task is formulated as the nonlinear programming (NLP) problem, cubic B-spline functions are used to discretize the time domain. A joint profile $q(t)$ is discretized as follows:

$$q(\mathbf{s}, \mathbf{P}, t) = \sum_{i=1}^{m} \mathrm{N}_i(\mathbf{s}, t)\, P_i \qquad 0 \le t \le T \tag{3.1}$$

where $\mathbf{s} = \{s_0, \ldots, s_l\}$ is the knot vector, $\mathbf{P} = \{P_1, \ldots, P_m\}$ is the control point vector, and $\mathrm{N}_i(\mathbf{s}, t)$ is the basis function. The control points become the optimization design variables. As a result, $\mathbf{P}_{human1}$, $\mathbf{P}_{human2}$, and $\mathbf{P}_{box}$ are the design variables for the human1, human2, and the box, respectively. Note that the box global joints represent two global translations and one global rotation. In addition, the grasping forces ($\mathbf{f}_1^c$ and $\mathbf{f}_2^c$) between human and box are also treated as design variables.

3.2.2 Objective functions

The dynamics effort (Xiang et al., 2010b) is used as the objective function for the team lifting motion which is defined as the summation of time integral of the squares of all joint torques for human1 and human2.

$$J(\mathbf{P}_{human1}, \mathbf{P}_{human2}, \mathbf{P}_{box}, \mathbf{f}_1^c, \mathbf{f}_2^c) = \sum_{i=1}^{n} \int_0^T \{\tau_{i(human1)}^2(\mathbf{P}_{human1}, \mathbf{f}_1^c) + \tau_{i(human2)}^2(\mathbf{P}_{human2}, \mathbf{f}_2^c)\} dt \quad (3.2)$$

where T is the total time. The total time duration T is a specified input parameter. Also, note that the joint torque for each human global DOF is zero for a balanced lifting motion.

3.2.3 Constraints

Two types of constraints are considered for the team lifting optimization problem: time dependent and time independent. Time dependent constraints include (1) joint angle limits, (2) torque limits, (3) feet contacting position, (4) dynamic stability, (5) collision avoidance, (6) box forward, (7) box range of motion, (8) box grasping, (9) box global EOM. Time independent constraints include (10) initial and final box locations, (11) static conditions at the beginning and end of the motion, and (12) initial, mid-time, and final joint angles of knee, spine, and elbow. For time dependent constraints, constraints (1-6) are imposed for both human1 and human2, and constraints (7-9) are imposed for the box.

Time dependent constraints are calculated sequentially in the optimization process at every time discretization point. From Figure 3.2, it is seen that at time t_1, the optimization first calculates all the time dependent constraints for human1. After that, the optimization proceeds the calculation for the constraints of human2, and lastly, it will calculate the constraints for the box. This loop will continue until the final time point T. In contrast, the optimization calculates the time independent constraints for human1 and human2 at a specific time.

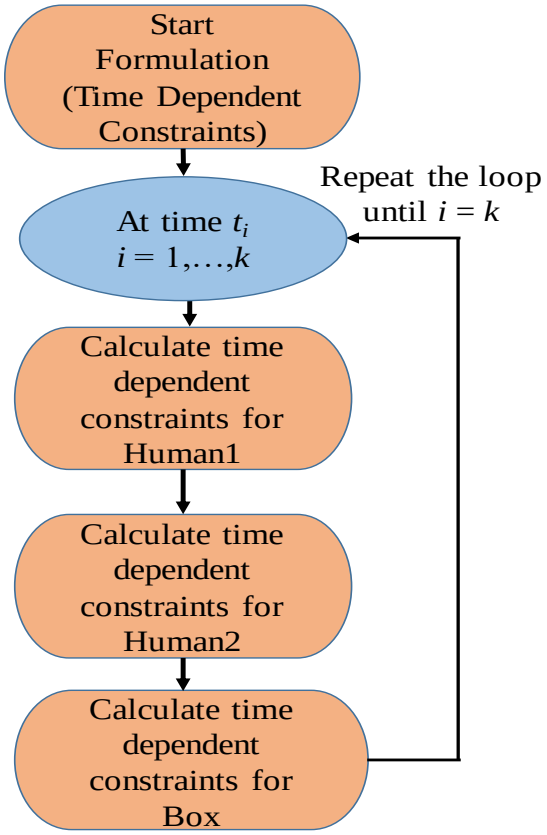

Figure 3.2 Calculation of time dependent constraints

3.2.3.1 Time dependent constraints

(1) Joint angle limits

$$\mathbf{q}_{human1}^{L} \leq \mathbf{q}_{human1}(t) \leq \mathbf{q}_{human1}^{U} \tag{3.3}$$

$$\mathbf{q}_{human2}^{L} \leq \mathbf{q}_{human2}(t) \leq \mathbf{q}_{human2}^{U}$$

where $\mathbf{q}_{human1}^{L}$ and $\mathbf{q}_{human2}^{L}$ are the lower joint angle limits, and $\mathbf{q}_{human1}^{U}$ and $\mathbf{q}_{human2}^{U}$ are the upper joint limits for human1 and human2, respectively.

(2) Joint torque limits

$$\boldsymbol{\tau}_{human1}^{L} \leq \boldsymbol{\tau}_{human1}(t) \leq \boldsymbol{\tau}_{human1}^{U} \tag{3.4}$$

$$\boldsymbol{\tau}_{human2}^{L} \leq \boldsymbol{\tau}_{human2}(t) \leq \boldsymbol{\tau}_{human2}^{U}$$

where $\boldsymbol{\tau}_{human1}^{L}$ and $\boldsymbol{\tau}_{human2}^{L}$ are dynamic lower joint torque limits, and $\boldsymbol{\tau}_{human1}^{U}$ and $\boldsymbol{\tau}_{human2}^{U}$ are dynamic upper limits for human1 and human2 (Xiang et al. 2019), respectively.

(3) Feet contacting positions

$$p_{human1\_feet}(t) = p_{human1\_feet}^{s}$$
$$p_{human2\_feet}(t) = p_{human2\_feet}^{s} \tag{3.5}$$

where $p_{human1\_feet}^{s}$ and $p_{human2\_feet}^{s}$ are the specified feet contact position on the level ground.

(4) Dynamic stability/Balance condition

$$p_{human1\_ZMP}(t) \in \text{FSR}$$
$$p_{human2\_ZMP}(t) \in \text{FSR} \tag{3.6}$$

where ZMP position is inside the foot support region (FSR) for human1 and human2 as shown in Figure 3.3.

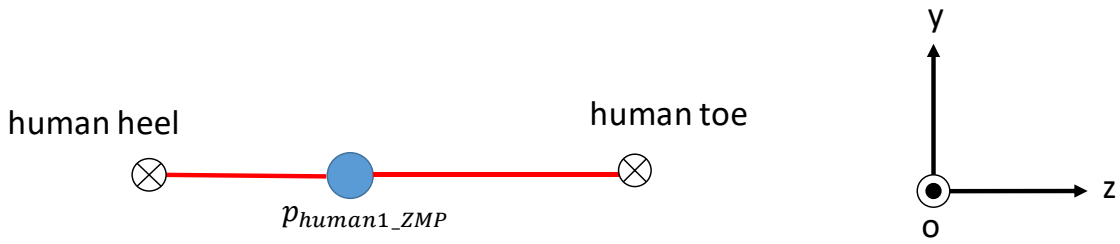

Figure 3.3 Foot support region

(5) Collision avoidance

$$d_{human1}(t) \geq r_{human1}$$
$$d_{human2}(t) \geq r_{human2} \tag{3.7}$$

where d_{human1} and d_{human2} are the calculated distance between the hand and the circle center on body segment representing the body thickness, can be expressed as $d_{human1} = \frac{\|\mathbf{r}_{\text{human1\_body}} \times \mathbf{r}_{\text{box\_edge}}\|}{\|\mathbf{r}_{\text{box\_edge}}\|}$, r_{human1} and r_{human2} are the radius of the circle for human1 and human2 as shown is Figure 3.4. There are total seven circles for each human model filled into body segments: two for spine and five for leg.

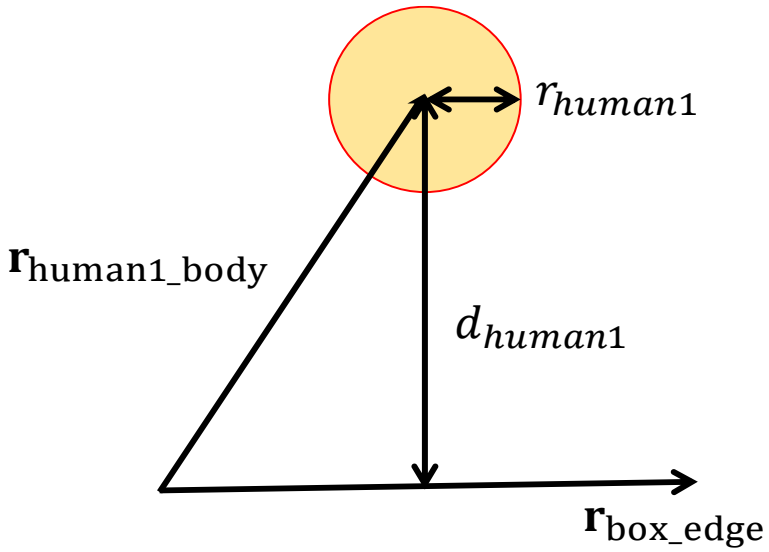

Figure 3.4 Collision avoidance constraint between the box and human body

(6) Box forward

$$Z_{human1\_wrist}(t) - Z_{human1\_pelvis}(t) \geq 0 \tag{3.8}$$

where Z_{human1_wrist} and Z_{human1_pelvis} are the global Z coordinates of wrist and pelvis points of human1 as shown in Figure 3.5.

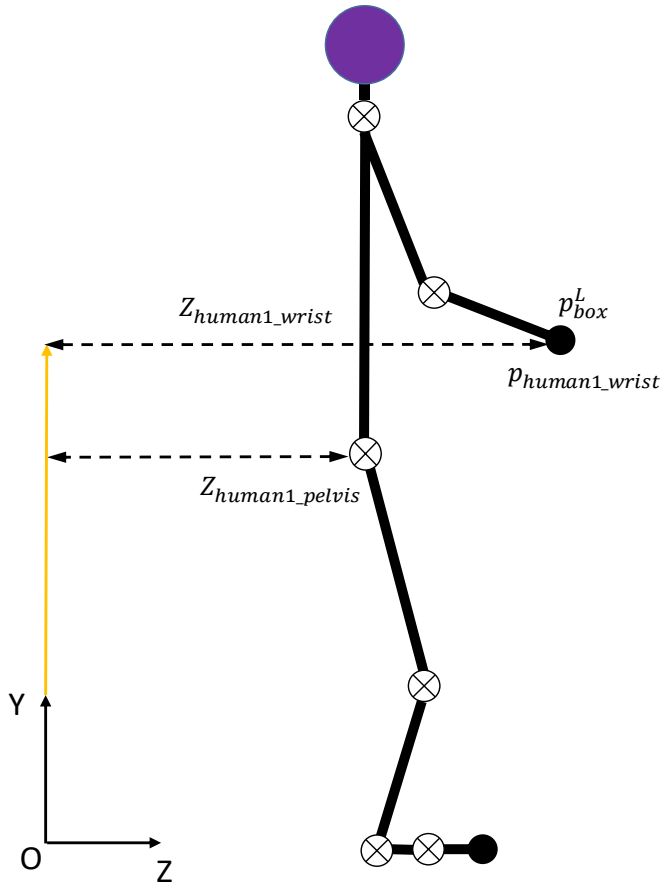

Figure 3.5 Box forward and box grasping constraints

(7) Box range of motion

$$\mathbf{q}^L_{box} \leq \mathbf{q}_{box}(t) \leq \mathbf{q}^U_{box} \tag{3.9}$$

where $\mathbf{q}^L_{box}$ is the lower box joint angle limits and $\mathbf{q}^U_{box}$ is the upper limit.

(8) Box grasping

$$p_{human1\_wrist}(t) - p^L_{box}(t) = 0 \tag{3.10}$$

$$p_{human2\_wrist}(t) - p^R_{box}(t) = 0$$

where p_{human1_wrist} and p_{human2_wrist} are the wrist positions of human1 and human2, respectively. p^L_{box} and p^R_{box} are the left and right edge positions of the box as shown in Figure 3.5.

(9) Box EOM

$$\left|\tau_i^{box}\right| \leq \varepsilon, \qquad i = 1,2,3 \tag{3.11}$$

where $\boldsymbol{\tau}_{box}$ is the global joint force and torque values of the box, $\varepsilon = 1$ N. Two external grasping forces are acting on the box edges to keep it in balance as shown in Figure 3.6. Also, GRF1 and GRF2 acting on human1 and human2 keep the human-box system in balance.

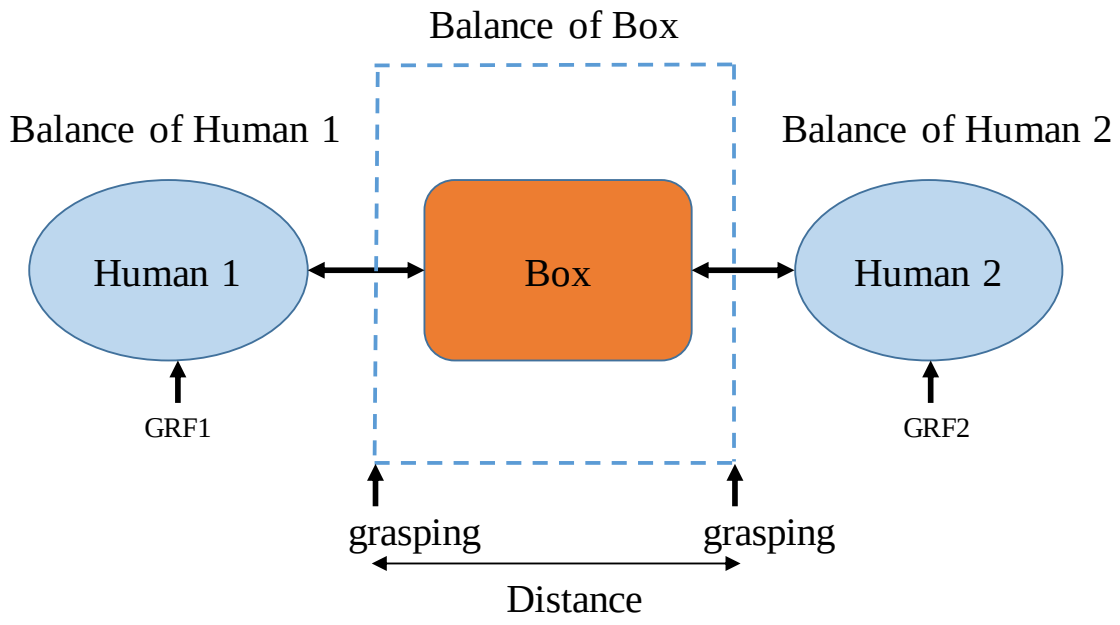

Figure 3.6 Box EOM constraint

3.2.3.2 Time independent constraints

(10) Initial and final hand positions

$$p_{human1\_hand}(t) = p^s_{human1\_hand}(t); \qquad t = 0, T \tag{3.12}$$

$$p_{human2\_hand}(t) = p^s_{human2\_hand}(t)$$

where, $p^s_{human1\_hand}$ and $p^s_{human2\_hand}$ are the specified hand positions at initial and final times.

(11) Initial and final static conditions

$$\ddot{\mathbf{q}}_{human1}(t) = \mathbf{0}; \qquad t = 0, T \tag{3.13}$$

$$\ddot{\mathbf{q}}_{human2}(t) = \mathbf{0}$$

$$\ddot{\mathbf{q}}_{box}(t) = \mathbf{0}$$

(12) Initial, mid-time, and final joint angles for knee, spine, and elbow

$$\left|q_{i\_human1}(t) - q^{E}_{i\_human1}(t)\right| \leq 10^{\circ}; \qquad t = 0, \frac{T}{2}, T \tag{3.14}$$

$$\left|q_{i\_human2}(t) - q^{E}_{i\_human2}(t)\right| \leq 10^{\circ}$$

where q_i^E is the experimental joint angle for knee, spine, and elbow joints.

CHAPTER IV

NUMERICAL RESULTS

A sequential quadratic programming (SQP) algorithm in SNOPT (Gill et al., 2002) is used to solve the nonlinear optimization problem of team lifting. To use the algorithm, cost and constraint functions and their gradients need to be calculated. The recursive kinematics and dynamics provide accurate gradients to improve the computational efficiency of the optimization algorithm (Xiang et al., 2009b; Lee et al., 2005). $\mathbf{P} = [\mathbf{P}_{human1}, \mathbf{P}_{human2}, \mathbf{P}_{box}] = \mathbf{0}$, $\mathbf{f}_1^c = \mathbf{f}_2^c = \mathbf{10}$ are used as the initial guess for the optimization. There are total 168 design variables and 1146 nonlinear constraints. The adaptive lifting strategies are predicted for team lifting by solving the NLP problem. The optimal solution is obtained in 151.99 seconds on a laptop with an Intel® Core™ i7 2.11 GHz CPU and 16 GB RAM. The input data related to the team box-lifting task (refer to Figure 3.1) are given in Table 4.1.

Table 4.1 Task parameters for the box team lifting

Parameters	
Board weight (Kg)	10
Board width (m)	0.370
Board height (m)	0.05
Board depth (m)	0.5
$d_1 = d_2$ (m)	0.375
$h_1 = h_3$ (m)	0.073
$d_3 = d_4$ (m)	0.875
$h_2 = h_4$ (m)	1.0
Standing distance, L(m)	1.25
T (s)	2.0

4.1 Case 1: Centric-weight lifting simulation

In this case, the box COM is in the middle, and other parameters are listed in Table 3.1 (centric-weight lifting). The joint torque, GRF, and hand-box grasping force profiles for centric-weight team lifting are presented in Figures 4.1- 4.3, respectively.

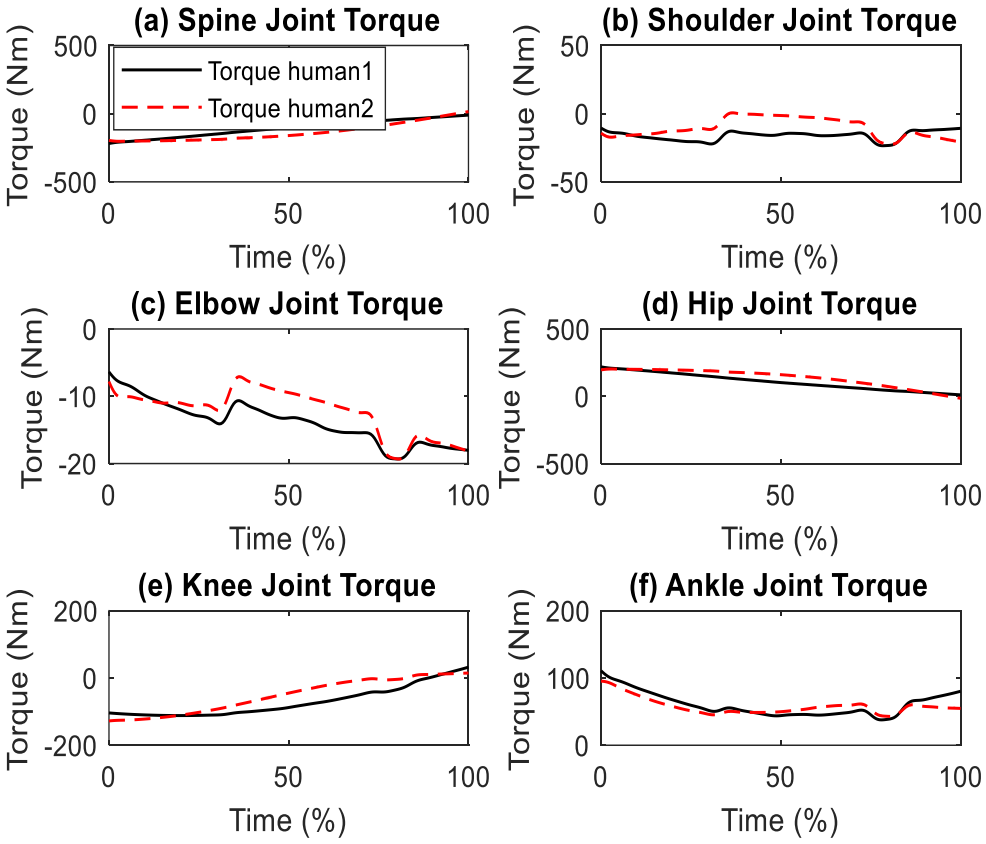

Figure 4.1 Comparison of centric-weight lifting joint torque profiles

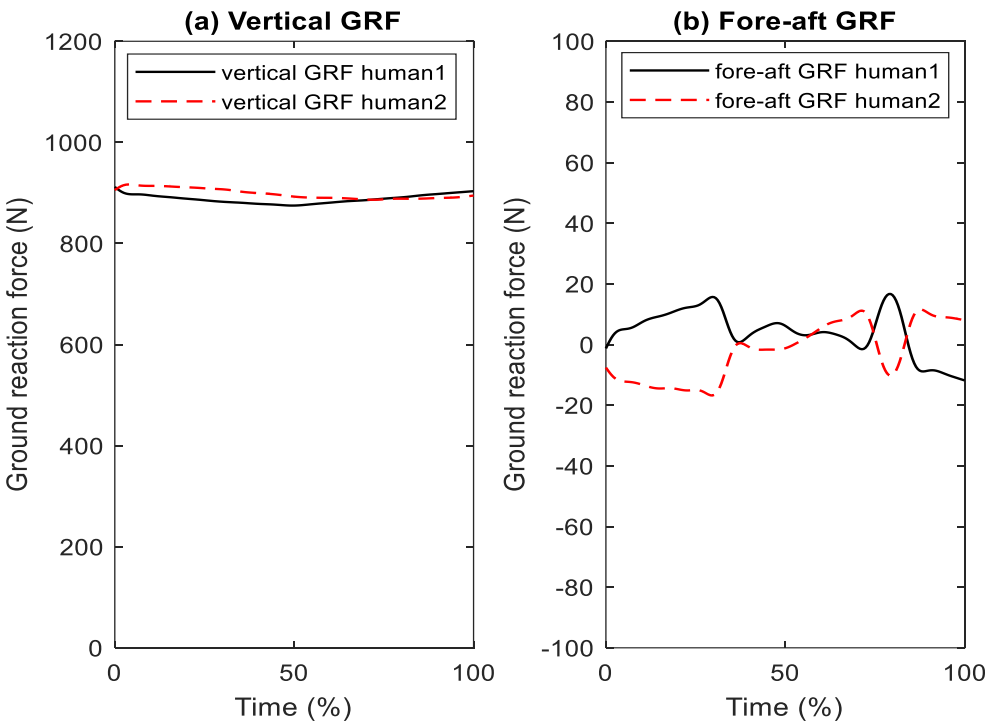

Figure 4.2 Comparison of centric-weight lifting GRF profiles

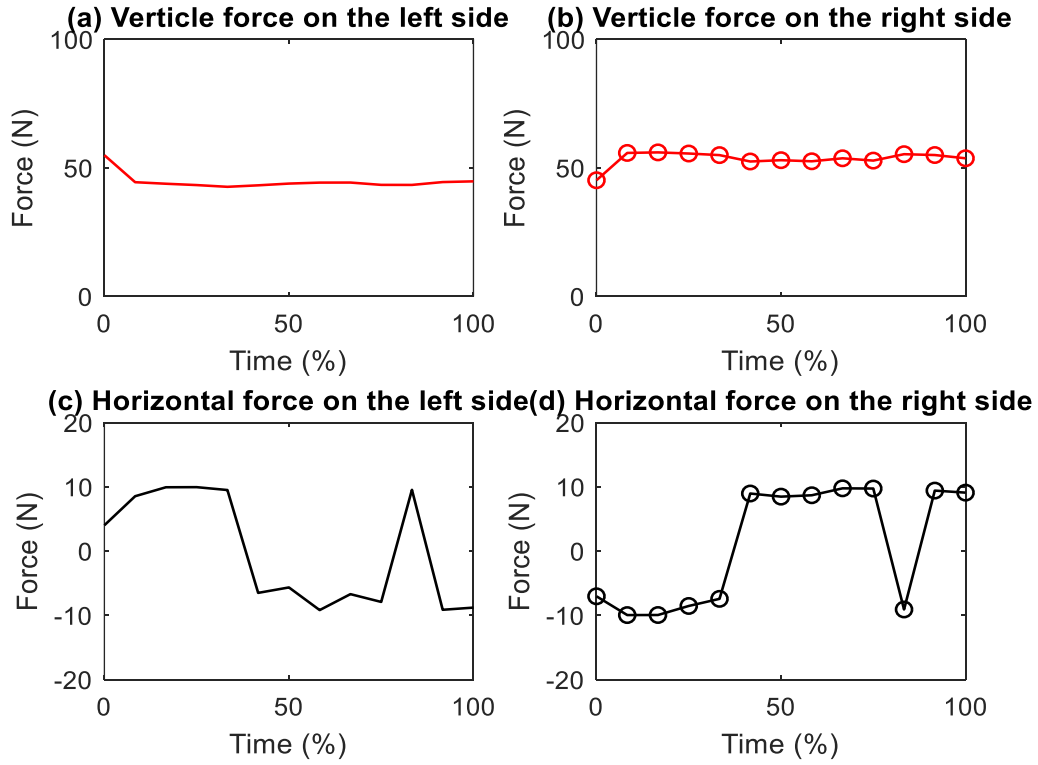

Figure 4.3 Hand-box grasping forces for centric-weight lifting

4.2 Case 2: Eccentric-weight lifting simulation

In this case, the effects of the box's COM location on the dynamic lifting motion are studied. We move the box's COM 0.1m towards human2 in the horizontal direction while other parameters are the same in Table 4.1. The joint torque, GRF, and hand-box grasping force profiles for eccentric-weight team lifting are presented in Figures 4.4 - 4.6, respectively.

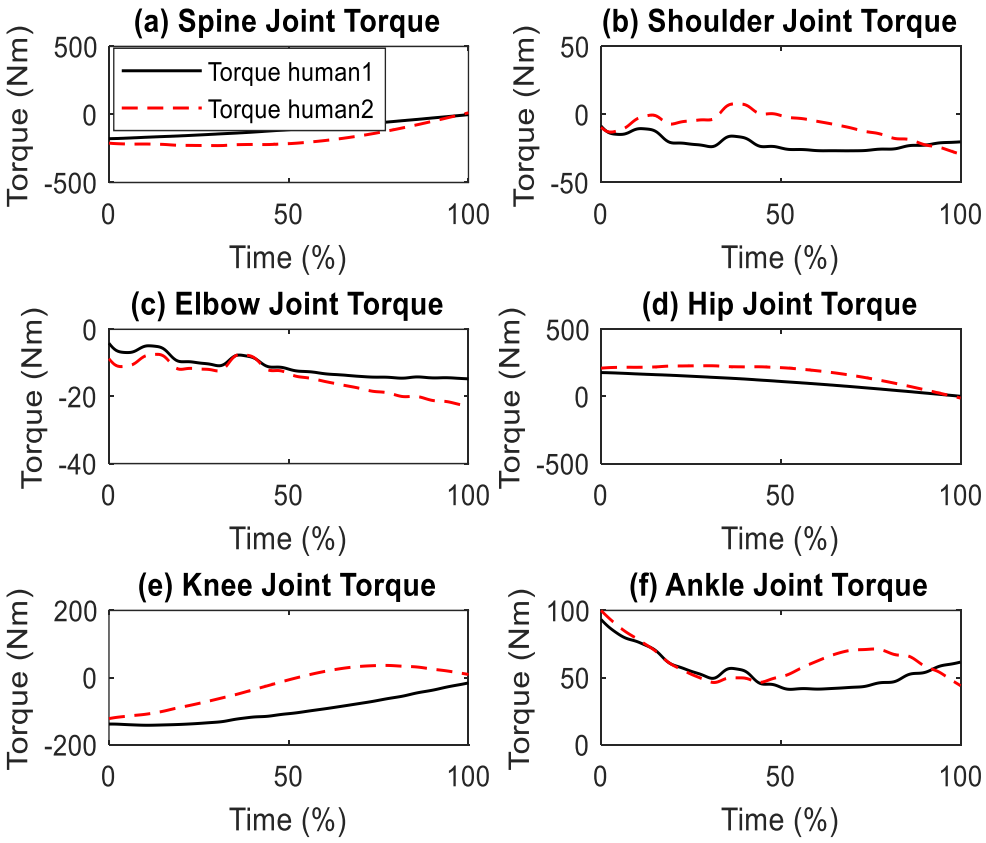

Figure 4.4 Comparison of eccentric-weight lifting joint torque profiles

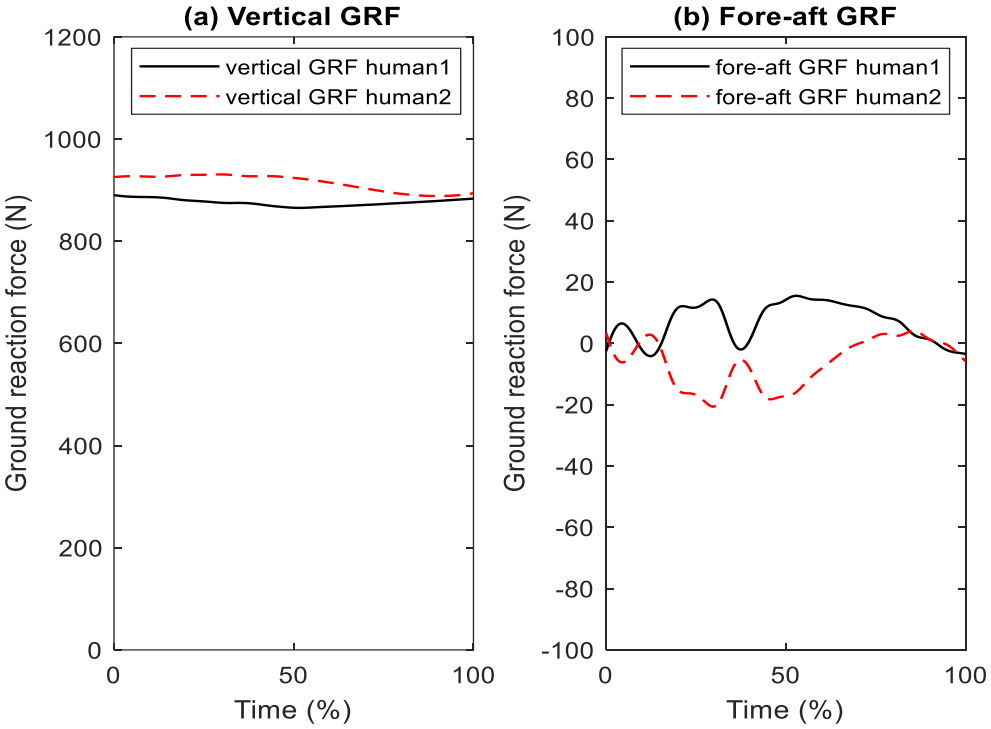

Figure 4.5 Comparison of eccentric-weight lifting GRF profiles

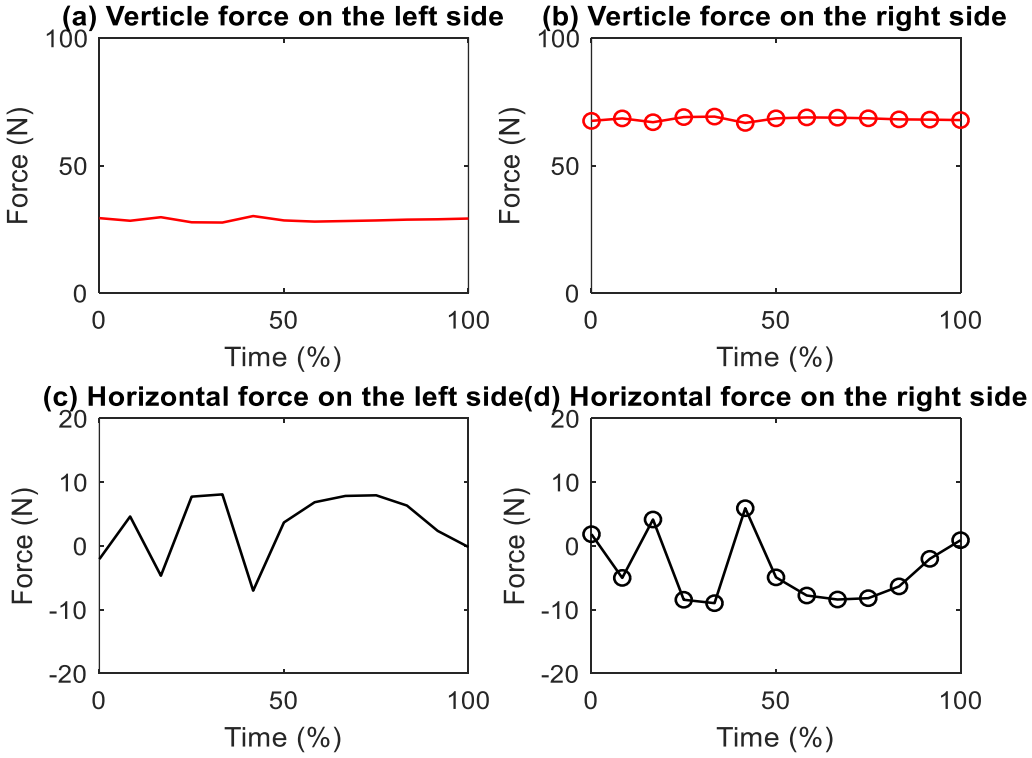

Figure 4.6 Hand-box grasping forces for eccentric-weight lifting

4.3 Validation

Two college students with 50th percentile height and weight are recruited for team lifting experiment in this study. The subjects have no musculoskeletal disorders and specific training in MMH techniques. The team lifting experiments are approved by the Institutional Review Board (IRB) of Oklahoma State University. Two team lifting tasks, centric-weight, and eccentric-weight, are performed, and each team lifting task is repeated three times with 5 seconds rest between two consecutive liftings. Canon EOS Rebel T7i DSLR Camera is used to record the videos of each team lifting task.

Kinovea (Anguilar et al., 2015), a video analysis software, is used to track the ankle, knee, hip, spine, elbow, and wrist marker positions of human1 and human2 during the team lifting motion as shown in Figure 4.8 (a, b). It will be possible to track the marker's route from start to finish by selecting the option called Track Path in Kinovea. Then the Cartesian coordinates of these markers are output to calculate the knee, hip, spine, and elbow joint angles using the trigonometry formula. Finally, MATLAB® is used for postprocessing (average and resampling) the output data to obtain the joint angle graphs for human1 and human2. The whole process is shown in Figure 4.7 and this flow is repeated for each video.

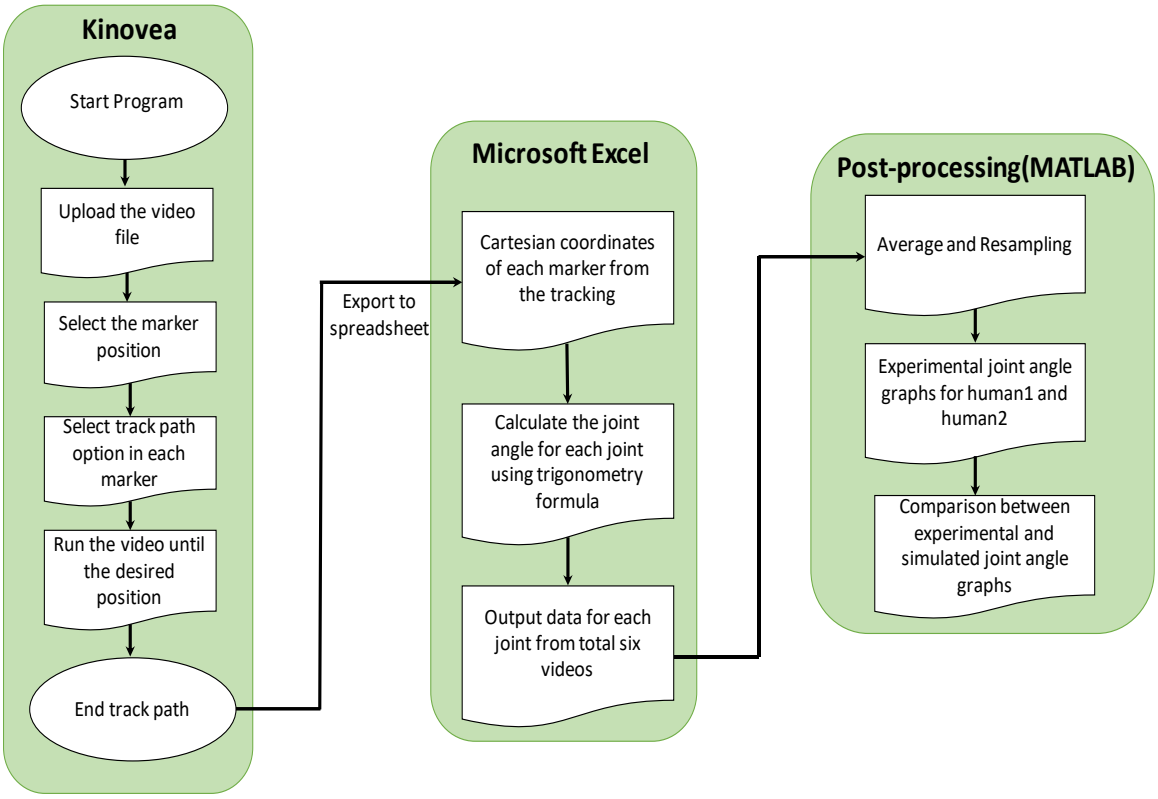

Figure 4.7 Flowchart of the experimental procedure

The simulated motion is validated against the experimental joint angle profiles in Figures 4.9 and 4.10 for centric- and eccentric-weight liftings, respectively.

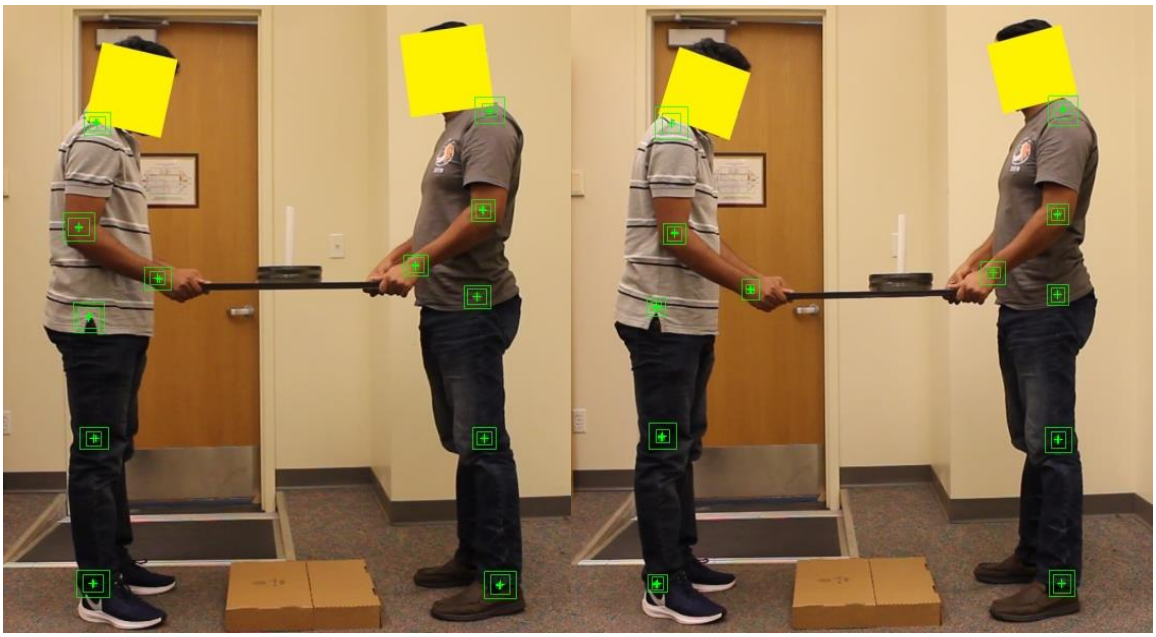

(a) (b)

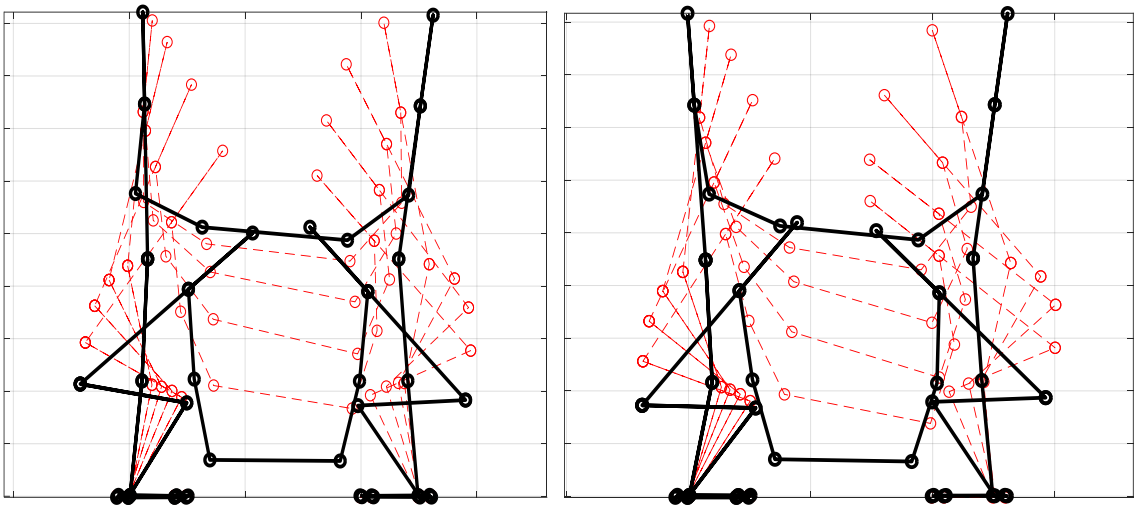

(c) (d)

Figure 4.8 Team lifting motion for 10 Kg box: (a) Centric-weight experiment, (b) eccentric-weight experiment, (c) centric-weight simulation, (d) eccentric-weight simulation

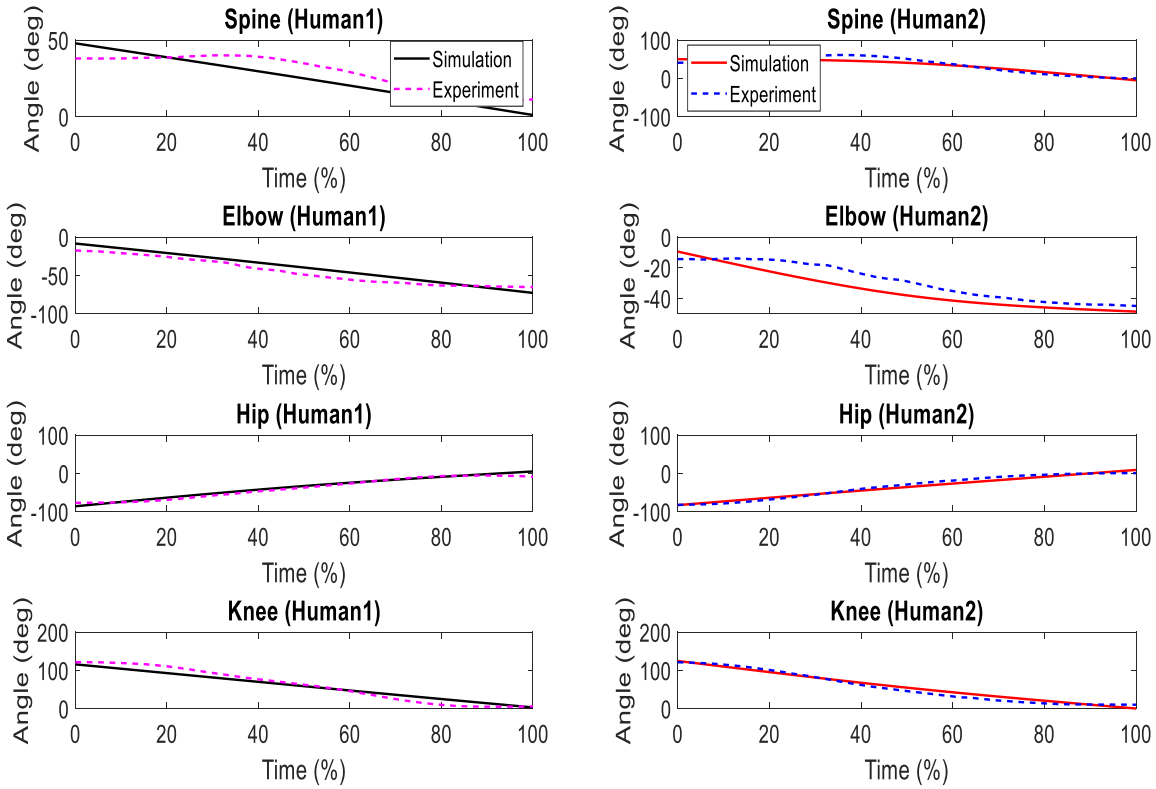

Figure 4.9 Joint angle profile validation for centric-weight team lifting

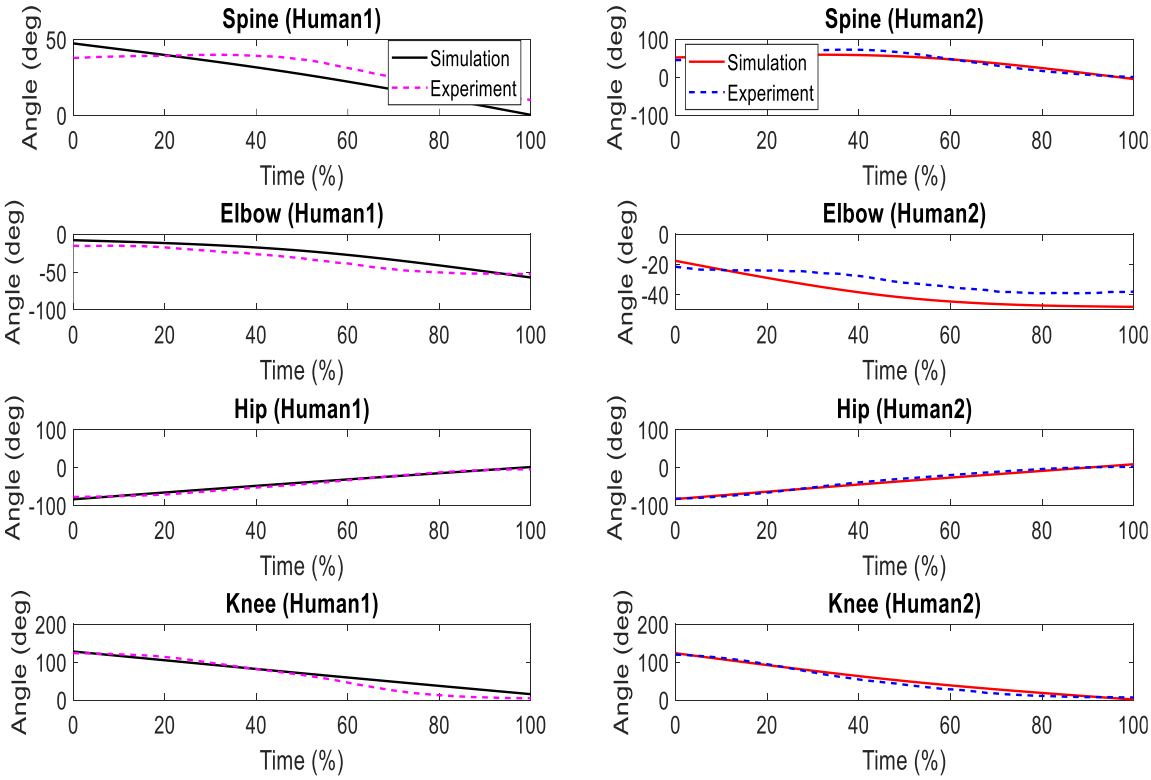

Figure 4.10 Joint angle profile validation for eccentric-weight team lifting

4.4 Discussion

For case 1, the box COM is in the middle. The lower body (hip, knee, and ankle) joint torques are similar for human1 and human2, as shown in Figure 4.1. However, the upper body (spine, shoulder, and elbow) joint torques are different. Human1 has a small spine torque but large shoulder and elbow torques. This reflects different lifting strategies for two team members. For GRF profiles in Figure 4.2, the vertical GRFs for human1 and human2 have similar magnitudes and trends. The summation of human1 and human2's horizontal GRFs is approximately equal to zero to keep the system in balance in the horizontal direction. For hand-box grasping forces, the vertical grasping forces for human1 and human2 are similar and roughly half of the box weight, and the horizontal grasping force values are in opposite directions to keep the box in balance as shown in Figure 4.3.

For case 2, we can see the differences of joint torque, GRF, and grasping force profiles between human1 and human2 as depicted in Figures 4.4-4.6. The vertical GRF for human2 is larger than that of human1. Like centric-weight team lifting, the summation of human1 and human2's horizontal GRFs for eccentric-weight team lifting is approximately equal to zero as shown in Figure 4.5. For the grasping forces in Figure 4.6, human2 takes more vertical weight than human1 because the weight location is close to human2. In addition, the summation of the vertical grasping forces is approximately equal to the weight of the box. The horizontal grasping forces have similar magnitudes but in opposite directions. It is interesting to note that human1 has larger lower body joint torques than human2. In contrast, human2 has a larger spine and elbow joint torques during eccentric-weight lifting as shown in Figure 4.4.

The snapshots of the predicted lifting are depicted in Figure 4.8 (c, d). It is seen that the initial squat postures of human1 and human2 are similar, but the final standing postures are different,

especially the arm postures. For eccentric-weight lifting, human2 pulls the box close to his body at final standing posture because the eccentric weight is on his side. For centric-weight lifting, the two final postures are quite similar. We can also see from Figure 4.8(d) that human2 uses a different lifting strategy compared to human1. In the beginning, human2 raises his hip first, then extends the knee. In contrast, human1 starts from knee extension directly. Therefore, the box is not strictly parallel to the ground, and there is a small rotation during the lifting process.

The centric and eccentric-weight lifting joint angle profiles are validated with video capture experiments in Figures 4.9 and 4.10, respectively. It is seen that the joint angle of spine, elbow, hip, and knee have similar trends and magnitudes as the experimental data. We impose joint angle constraints for knee, spine, and elbow at initial, mid-time, and final time points. It is necessary to impose these time-independent constraints because human1 and human2 have different lifting strategies (Xiang et al., 2010c). It is noted that we only impose joint angle constraints on several key joints to predict team lifting motion. It has been demonstrated that other joints' angle profiles (ankle, hip, and shoulder) are successfully predicted without imposing joint angle constraints.

During the team lifting, the most common injury is low back injury due to spinal loading. This injury can be predicted based on the injury index for spine joint torques. The ratio of the current joint torque to the joint torque limits is called the injury index of that joint. When the injury index is close to 1 for any joint, then the joint tends to face injury. In this study, from the simulation and experiment data, both for centric and eccentric weight lifting, the injury index for spine joint torques is not close to 1 for human1 and human2, respectively. So the spine joints are free from injury both for human1 and human2. Therefore, the simulated motion can be considered as a safe motion. In addition, using this optimization approach and musculoskeletal model, one can find the optimal joint angle and muscle forces to minimize a muscle-related cost function subjected to physical and task-based constraints. Also, in conjunction with the predicted motion, one can then

conduct a finite element analysis of a muscle for predicting muscle strain injury during team lifting.

In this study, joint profiles were discretized using cubic B-splines, and five control points were used to represent each DOF for a joint angle profile. The total time duration is discretized into two evenly distributed segments, and each segment has six discretization points, so a total 13 discretized output points. It was chosen based on the numerical test performed for the optimization. It was concluded that 13 discretized output points give an optimal solution successfully and quickly. It is also noted that if we increase the total number of discretized output points, there will be more control points, and more constraints need to be calculated which is difficult to converge and computationally inefficient.

CHAPTER V

CONCLUSIONS AND FUTURE WORK

5.1 Conclusions

In this study, a novel optimization-based multibody dynamics modeling method was proposed to predict team lifting motion and hand grasping forces. Reasonable simulation results were obtained. Denavit-Hartenberg (DH) method was used to express the kinematics and dynamics of mechanical joints of human and box. The floating-base box with grasping forces was used to model human-box interaction. The team lifting problem was formulated as an NLP optimization problem and efficiently solved using a gradient-based optimizer SNOPT (Gill et al., 2002). The effect of box COM was investigated. The simulation demonstrated that the box COM location has significant effects on the optimal team lifting strategy, kinematics, and kinetics. Two college students with 50^{th} percentile height and weight have performed the team lifting task, and the simulated motion is validated against the experimental joint angle profiles. These results can be used to plan the optimal team lifting motion to prevent injury.

5.2 Future Work

Besides the foregoing work, the following issues will be studied in the future:

(1) extending the 2D skeletal lifting model to 3D model; (2) extending the skeletal model to musculoskeletal model; (3) conducting more rigorous motion capture validation; (4) further extending this work to human-robot interaction for team lifting; (5) delivering an ergonomic tool to prevent spine injury for team lifting.

5.2.1 Motion capture validation

The most immediate continuation of this research would be more rigorous motion capture validations. We plan to recruit 20 subjects to conduct team lifting experiments. Also, the effects of different box weight on team lifting motion prediction will be studied.

5.2.2 2D skeletal lifting model to 3D model

Another the most immediate continuation of this research would be to expand the 2D model to a 3D model. The progression to a 3D model would increase the complexity due to its expansion of DOFs and a new axis of movement.

5.2.3 Skeletal model to musculoskeletal model

The simulation in this study is based on 2D skeletal model in joint space. The major advantage of the skeletal model is its computational efficiency. However, it excludes the important muscle activity and recruitment information. The optimization of a musculoskeletal model can be burdensome. The recently developed numerical methods, such as inverse dynamics based optimization and collocation method, will be used for musculoskeletal team lifting simulation.

5.2.4 Human-robot interaction for team lifting

Human-robot collaboration has a wide range of applications and high economic impact. Over the past years, researchers have developed different frameworks and methodologies to perform human-robot team lifting tasks. The proposed human team lifting prediction method can be used to study human-robot team lifting problems. Our goal is to use the predictive dynamics method developed in this thesis to predict human and robot motions, then use controllers to control the robot behavior.

5.2.5 Ergonomic tool to prevent spine injury

An ergonomic tool will be delivered to prevent spine injury based on the simulation model developed in this study. The spine torque injury index is defined as the ratio of the current calculated spine torque to the spine torque limit. If spine injury index is close to 1, it indicates a dangerous lifting situation. A threshold should be set for spine torque injury index to prevent spine injury for team lifting. The developed tool can output injury index during the dynamic lifting process to access injury conditions. Finally, this real-time simulation software will be delivered as an ergonomic tool to prevent injury for lifting.

REFERENCES

Aberg, U., Elgstrand, K., Magnus, P., & Lindholm, A., 1967, Analysts of components and prediction of energy expenditure in manual tasks. The International Journal of Production Research, 6(3), 189-196.

Ackermann, M., & Van den Bogert, A.J., 2010, Optimality principles for model-based prediction of human gait. Journal of Biomechanics, 43(6), 1055-1060.

Aguilar, L.M., Torres, J.P., Jimenes, C.R., Cabrera, D.R., Cárdenas, M.F., Urgirles, P.F., 2015, Analysis of the angles in hip, knee and ankle during the pedaling of a Cross Country Olympic cyclist. 2015 CHILEAN Conference on Electrical, Electronics Engineering, Information and Communication Technologies (CHILECON), October 28-30, Santiago, Chile, pp205-208.

Aquilano, N. J., 1968, A physiological evaluation of time standards for strenuous work as set by stopwatch time study and two predetermined motion time data systems, Journal of Industrial Engineering, 19, 425-432.

Arisumi, H., Chardonnet, J. R., Kheddar, A., and Yokoi, K., 2007, Dynamic lifting motion of humanoid robots, 2007 IEEE International Conference on Robotics and Automation, Roma, Italy, pp. 2661-2667.

Arora, J., & Wang, Q., 2005, Review of formulations for structural and mechanical system optimization. Structural and Multidisciplinary Optimization, 30(4), 251-272.

Astrand, P. O., and Rodahl, K., 1986, Textbook of Work Physiology, 3rd edition. New York: McGraw-Hill.

Ayoub, M. M., Bethea, N. J., Bobo, M., Burford, C. L., Caddel, K., Intaranont, K., et al., 1981, Mining in Low Coal, Vol. 1, Biomechanics and Work Physiology, Final Report, US Bureau of Mines, Contract No. H03087022.

Ayoub, M., 1992, Problems and solutions in manual materials handling: the state of the art. Ergonomics, 35(7-8), 713-728.

Chaffin, D.B., Andersson G.B.J., Martin, B.J., 1999. Occupational Biomechanics, 3rd Edition. John Wiley & Sons, New York, NY, 233, 318, 319.

Charney, W., Zimmerman, K. and Walara, E., 1991, The lifting team: A design method to reduce lost time back injury in nursing. American Association of Occupational Health Nurses, 35**,** 231-234.

Cheng, F.T., and Orin, D.E., 1991, Efficient formulation of the force distribution equations for simple closed-chain robotic mechanisms. IEEE Transactions on System, Man, and,

Cybernetics,21(1), 25-32.

Cheng, H., Obergefell, L., and Rizer, A., 1994, Generator of body (GEBOD) manual, AL/CF-TR-1994-0051, Armstrong Laboratory, Wright-Patterson Air Force Base, Ohio.

Daynard, D., Yassi, A., Cooper, J. E., Tate, R., Norman, R., and Wells, R., 2001, Biomechanical analysis of peak and cumulative spinal loads during simulated patient handling activities: a substudy of a randomized controlled trial to prevent lift and transfer injury of health care workers. Applied Ergonomics, 32, 199-214.

DelPreto, J., and Rus, D., 2019, Sharing the load: human-robot team lifting using muscle activity, in 2019 IEEE International Conference on Robotics and Automation (ICRA), May 20-24, Montreal, Canada.

Denavit, J, and Hartenberg, RS, 1955, A kinematic notation for lower-pair mechanisms based on matrices, Journal of Applied Mechanics, 22, 215-221.

Dennis, G.J., & Barrett, R.S., 2003, Spinal loads during two-person team lifting: Effect of matched versus unmatched standing height. International Journal of Industrial Ergonomics, 32(1), 25-38.

Durnin, J. V. G. A., and Passmore, R., 1967, Energy, Work and Leisure, London: Heinemann Educational.

Farahani, S. D., Andersen, M. S., de Zee, M., & Rasmussen, J., 2016, Optimization-based dynamic prediction of kinematic and kinetic patterns for a human vertical jump from a squatting position. Multibody System Dynamics, 36(1), 37-65.

Frederik, W., 1959, Human energy in manual lifting. Modern Materials Handling, 14(3), 74-76.

Fox, R.R., 1982, A psychophysical study of bimanual lifting. Master's thesis, Texas Tech, Lubbock, TX.

Fregly, B. J., Reinbolt, J. A., Rooney, K. L., Mitchell, K. H., & Chmielewski, T. L., 2007, Design of patient-specific gait modifications for knee osteoarthritis rehabilitation. IEEE Transactions on Biomedical Engineering, 54(9), 1687-1695.

Gill, P.E., Murray, W., and Saunders, M.A., 2002, SNOPT: An SQP algorithm for large-scale constrained optimization. SIAM Journal of Optimization, 12(4), 979-1006.

Hamilton, B. J., and Chase, R. B., 1969, A work physiology study of the relative effects of pace and weight in a carton handling task, Transactions of the American Institute of Industrial Engineers, 1, 106-111.

Johnson, S., & Lewis, D., 1989, A psychophysical study of two-person manual materials handling tasks. In the Proceedings of the Human Factors Society 33rd Annual Meeting, 651-653. Santa Monica, CA, Human Factors Society.

Karwowski, W., & Mital, A., 1986, Isometric and isokinetic testing of lifting strength of males in teamwork. Ergonomics, 29(7), 869-878.

Karwowski, W., 1988, Maximum load lifting capacity of males and females in teamwork. In the Proceedings of the Human Factors Society 32nd Annual Meeting, 680-682. Santa Monica, CA, Human Factors Society.

Karwowski, W., & Pongpatanasuegsa, N., 1988, Testing of isometric and isokinetic lifting strengths of untrained females in teamwork. Ergonomics, 31(3), 291-301.

Konz, S.A., Johnson, S., 2004. Work Design Occupational Ergonomics, 6 th Edition. Holcomb Hathaway, Inc., Scottsdale, AZ, 230, 250, 258.

Lawitzky, M., Mörtl, A., and Hirche, S., 2010, Load sharing in human-robot cooperative manipulation. Proceedings of IEEE Ro-Man, 185-191.

Lee, K.S., & Lee, J.H., 2001, A study of efficiency of two-man lifting work. International Journal of Industrial Ergonomics, 28(3-4), 197-202.

Lee, S.H., Kim, J., Park, F.C., Kim, M., and Bobrow, J.E., 2005, Newton-type algorithm for dynamics-based robot movement optimization. IEEE Transactions on Robotics, 21(4), 657-667.

Marras, W.S., Davis, K.G., Kirking, B.C., & Granata, K.P., 1999, Spine loading and trunk kinematics during team lifting. Ergonomics, 42(10), 1258-1273.

Mital, A., 1984, Comprehensive maximum acceptable weight of lift database for regular 8-hour workshifts. Ergonomics, 27, 1127-1138.

Mital, A., & Motorwala, A., 1995, An ergonomic evaluation of steel and composite access covers. International Journal of Industrial Ergonomics, 15(4), 285-296.

Ren, L., Jones, R. K., & Howard, D., 2007, Predictive modelling of human walking over a complete gait cycle. Journal of Biomechanics, 40(7), 1567-1574.

Rice, V.J., Sharp, M.A., Nindl, B.C., & Bills, R.K., 1995, Prediction of two-person team lifting capacity. In the Proceedings of the Human Factors and Ergonomics 39th Annual Meeting, 645-649. Santa Monica, CA, Human Factors Society.

Sharp, M.A., Rice, V.J., Nindl, B.C., & Williamson, T.L. 1997, Effects of team size on the maximum weight bar lifting strength of military personnel. Human Factors, 39(3), 481-488.

Shourijeh, M. S., & McPhee, J., 2014, Forward dynamic optimization of human gait simulations: a global parameterization approach. Journal of Computational and Nonlinear Dynamics, 9(3), 031018.

Song, J., Qu, X., & Chen, C.H., 2016. Simulation of lifting motions using a novel multi-objective optimization approach. International Journal of Industrial Ergonomics, 53, 37-47.

Thelen, D. G., & Anderson, F.C., 2006, Using computed muscle control to generate forward dynamic simulations of human walking from experimental data. Journal of Biomechanics, 39(6), 1107-1115.

Vukobratovic and Borovac, 2004, Zero-moment point — thirty-five years of its life. International Journal of Humanoid Robotics, 1(1), 157-173.

Xiang, Y., Arora, J. S., Rahmatalla, S., & Abdel-Malek, K., 2009a, Optimization-based dynamic human walking prediction: One step formulation. International Journal for Numerical Methods in Engineering, 79(6), 667-695.

Xiang, Y., Arora, J. S., and Abdel-Malek, K., 2009b, Optimization-based motion prediction of mechanical systems: sensitivity analysis. Structural and Multidisciplinary Optimization, 37(6), 595-608.

Xiang, Y., Arora, J.S., and Abdel-Malek, K., 2010a, Physics-based modeling and simulation of human walking: a review of optimization-based and other approaches. Structural and Multidisciplinary Optimization, 42(1), 1-23.

Xiang, Y., Arora, J.S., Rahmatalla, S., Marler, T., Bhatt, R., Abdel-Malek, K., 2010b, Human lifting simulation using a multi-objective optimization approach, Multibody System Dynamics, 23(4), 431-451.

Xiang, Y., Chung, H.J., Kim, J.H., Bhatt, R., Rahmatalla, S., Yang, J., Marler, T., Arora, J.S., Abdel-Malek, K., 2010c, Predictive dynamics: an optimization-based novel approach for human motion simulation. Structural and Multidisciplinary Optimization, 41(3), 465-479.

Xiang, Y., Arora, J.S., & Abdel-Malek, K. 2012, 3D human lifting motion prediction with different performance measures. International Journal of Humanoid Robotics, 9(02), 1250012.

Xiang, Y., Zaman, R., Rakshit, R., and Yang, J., 2019, Subject-specific strength percentile determination for two-dimensional symmetric lifting considering dynamic joint strength, Multibody System Dynamics, 46(1), 63-76.

APPENDICES

Table A 1. Joint angle limits for human1 and human2

Joint name	Lower limit	Upper limit
Global translation 1 (forward) (m)	-5.0	5.0
Global translation 2 (upward) (m)	-5.0	5.0
Global rotation (degree)	-10.0	10.0
Spine (degree)	0.0	80.0
Shoulder (degree)	-90.0	90.0
Elbow (degree)	5.0	120.0
Hip (degree)	-90.0	90.0
Knee (degree)	5.0	120.0
Ankle (degree)	-20.0	80.0
Metatarsal (degree)	-50.0	20.0

Table A 2. Joint angle limits for Box

Joint name	Lower limit	Upper limit
Global translation 1 (forward) (m)	-5.0	5.0
Global translation 2 (upward) (m)	-5.0	5.0
Global rotation (degree)	-90.0	90.0

Table A 3. Static joint torque limits (Nm) for human1 and human2

Joint name	Lower limit	Upper limit
Global translation 1 (forward)	-500.0	500.0
Global translation 2 (upward)	-500.0	500.0
Global rotation	-500.0	500.0
Spine	-400.0	400.0
Shoulder	-184.0	126.0
Elbow	-117.4	120.6
Hip	-334.0	408.0
Knee	-518.2	206.4
Ankle	-75.4	170.6
Metatarsal	-140.0	140.0

Table A 4. Static joint torque limits (Nm) for Box

Joint name	Lower limit	Upper limit
Global translation 1 (forward)	-500.0	500.0
Global translation 2 (upward)	-500.0	500.0
Global rotation	-500.0	500.0

Table A 5. Box moment of inertia

Name	Moment of inertia ($Kg \cdot m^2$)
I_{xx}	0.00178645
I_{yy}	0.00364583
I_{zz}	0.00251328

Note that the arm and leg strength are doubled because arms and legs are modeled as single branches.

VITA

Md Asif Arefeen

Candidate for the Degree of

Master of Science

Thesis: AN OPTIMIZATION-BASED MULTIBODY DYNAMICS MODELING METHOD FOR TEAM LIFTING SIMULATION

Major Field: Mechanical Engineering

Biographical:

Education:

Completed the requirements for the Master of Science in Mechanical Engineering at Oklahoma State University, Stillwater, Oklahoma in December, 2019.

Completed the requirements for the Bachelor of Science in Aeronautical Engineering at Bangladesh University of Professionals, Dhaka, Bangladesh in 2015.

Experience:
Graduate Research Assistant, Biodynamics Optimization Laboratory, Oklahoma State University (August 2018- December 2019).

Graduate Teaching Assistant, University of Alaska Fairbanks (August 2017- May 2018).

Professional Memberships: N/A